Manuscript submitted to **Biophysical***Journal*
Article

Branching, crosslinking and decentralization of microtubules accelerates intracellular assembly

Apurba Sarkar[1], Alex Mogilner*[2], and Raja Paul*[1]

[1]School of Mathematical & Computational Sciences, Indian Association for the Cultivation of Science, Kolkata 700032, India
[2]Courant Institute and Department of Biology, New York University, New York, NY 10012, USA
*Correspondence: Correspondence to R.P. ssprp@iacs.res.in and A.M. mogilner@cims.nyu.edu

ABSTRACT Before cell division, mitotic spindle is assembled from chromosomes and centrosomes. After the cell division, Golgi organelles assemble from multiple vesicles scattered across daughter cells. These are among many other examples of intracellular assembly of vesicles, organelles and chromosomes made possible by dynamic microtubules. The most prominent microtubule networks are centrosome-focused asters that 'search' for the vesicles and chromosomes, but there are also microtubules originating from the vesicles and chromosomes, raising the question whether a coordination between multiple microtubule networks optimizes the assembly process. This study uses a computational model to examine how microtubule dynamics influence the assembly of organelles from vesicles. The model includes two microtubule populations: microtubules anchored to the vesicles, which drive local clustering, and 'central' microtubules anchored to the centrosome that aggregate the vesicles globally. Simulations show that a microtubule decentralization – balanced contribution from both microtubule populations — accelerates the assembly of tens of vesicles, but that assigning all microtubules to hundreds of vesicles optimizes the assembly. Directionally biased microtubule growth, particularly when avoiding spontaneous catastrophe events, further accelerates the assembly. Additionally, microtubule branching, when occurring at optimal angles and spacings, enhances the assembly's efficiency. Lastly, rapid crosslinking of overlapping central and 'local' microtubules can drastically accelerate the assembly. Applying this model to the spindle assembly in early mitosis reveals similar insights. The model suggests that the observed multiple microtubule networks optimize the intracellular assembly processes when molecular resources are limited.

SIGNIFICANCE Assembly of intracellular structures is a time-sensitive process driven by multiple dynamic microtubule networks. For example, vesicles must be aggregated by microtubules to form Golgi apparatus after cell division, while mitotic spindle assembly requires bringing chromosomes closer together by microtubules growing from spindle poles and chromosomes. Delays in these processes can lead to genomic instability and disease. Using modeling, we show how microtubules originating from centrosomes, vesicles, or chromosomes can be optimally distributed to minimize the assembly time. The model reveals roles of microtubule decentralization, branching and crosslinking in accelerating assembly. The model suggests that the intracellular assembly can be optimized by diversifying microtubule networks and enhancing their interactions.

INTRODUCTION

Assembly of organelles and other subcellular structures, i.e. fusion of mitochondria (1), is a crucial part of cell dynamics. Several such processes – reassembly of Golgi in daughter cells at the end of cell division (2), aggregation of melanosomes (pigment granules) in fish melanophore cells (3), and congression of chromosomes to mitotic spindle in prometaphase (4) – are driven by microtubules (MTs) and dynein motors. For example, to divide Golgi complex between daughter cells during cell division, Golgi stacks fragment into tens to thousands of vesicles that disperse stochastically across the cytoplasm in mitosis (5–7). As the mother cell transitions into telophase, these vesicles are gathered at centrosomes of the daughter cell, where the vesicles reassemble into Golgi stacks and ribbons (2).

This reassembly crucially depends on dynamic instability of MTs (8, 9), in which MT plus ends grow outward, then undergo a 'catastrophe', shrink inward, toward the MT organizing center (in this case centrosome), where MT minus ends are anchored, and then resume the growth after a 'rescue'. The catas-

trophes and rescues occur with certain frequencies at random times, and the resulting stochastic process effectively enables the MT plus ends to explore the cell volume. Namely, in an elementary act of the 'search-and-capture' process, a MT plus end growing in a random direction encounters a Golgi vesicle by sheer chance, dynein motors coating the vesicles transport it to the centrosome (10). A similar mechanism governs the central aggregation of pigment granules in melanophore cells (11). Last, but not least, accurate chromosome segregation during mitosis (12, 13) depends on mitotic spindle assembly that starts in early prometaphase with connecting chromosomes to two MT asters centered at two centrosomes. (Some cells opt for an alternative, centrosome-independent, spindle assembly pathway (14).) The early search-and-capture models posited that these connections are made by random contacts between the growing MT plus ends and kinetochores, small proteinaceous structures on the centromeres of the chromosomes (15).

The central, global search-and-capture process is usually complemented by a decentralized, local assembly made possible by nucleation and anchoring of MTs not only at the centrosomes, but also at the Golgi membranes (16) and pigment granules (11). MTs are also nucleated near and associate with kinetochores in complex and understudied ways (13, 17–20). Specifically, a non-centrosomal MT growing from one Golgi vesicle randomly encounters another such vesicle after which dynein motors on the second vesicle transport it toward the MT minus end on the first one, ending in merger of the two vesicles (10, 21). Similarly, melanophore pigment granules nucleate MTs (11, 22) that search randomly the cellular space, capture other pigment granules and bring the granules together in the dynein-dependent way (3, 11). While central and local aggregation processes could be sufficient on their own, they usually cooperate accelerating the assembly (3, 10, 11). This raises the broad question: *Is there an optimal strategy of the combined central-local MT-dynein-driven assembly, and if so, do cells in fact optimize the assembly?*

Furthermore, while chromosomes do not appear to aggregate locally, there is growing evidence that mitotic spindle assembly relies on interactions of long centrosomal MTs with short kinetochore MTs (23, 24). Namely, the direct kinetochore capture by centrosomal MTs is not the principal pathway of the spindle assembly, but rather either centrosomal MTs capture minus ends of kinetochore-associated short MTs, or the kinetochore MTs capture the centrosomal MT (4), after which bundles of the kinetochore MTs are pulled toward the centrosomes in a dynein-dependent way (17–20, 25, 26). Absence of the kinetochore MTs impedes the spindle assembly (27). Thus, like organelle assembly, spindle formation may also rely on a combined central-local search to optimize the spindle assembly.

The global and local searches in the spindle are further optimized by several factors, most prominently by making the searches less random and biasing MT growth towards chromosomes. The best understood relevant pathway is mediated by spatial gradients of RanGTP protein around chromosomes; this gradient increases capture probability by stabilizing MTs growth near chromosomes, preventing catastrophe before capture (28–30). Additional factor that can accelerate the search is random chromosome movement during early prometaphase (31).

Centrosomal MTs and MTs anchored to organelles, vesicles and chromosomes are not the only MT networks in the cell. MTs are also nucleated at and branch from the sides of pre-existing MTs in a process mediated by Augmin and other proteins (23, 24, 32–34). This branching MT nucleation is considered to be the major source of spindle MTs (35), and acentrosomal spindles rely mainly on the branched MT architecture to self-assemble (36). In centrosomal spindles, MT branching is a part of the spindle formation: inhibiting centrosomal MTs increases MT branching near chromosomes, while disrupting Augmin-dependent MT formation enhances centrosomal MT nucleation (37, 38). This suggests not only cooperation among different MT networks in the assembly processes, but also that this cooperation proceeds under constrants of limited molecular resources, i.e. of a finite supply of tubulin (37, 38). This raises the second key question: *What is the optimal coordination between several MT networks for the subcellular assemblies?*

In this study, we use a computational model to simulate the assembly of cellular organelles and vesicles (vesicles hereafter) through a MT-driven search process achieved by both central searcher MTs, originating from a single centrosome, and local searcher MTs produced by the vesicles. We quantify the roles of these two populations and examine potential contributions of MT branching, spatial and angular biases of MT growth, and MT crosslinking. We then apply a similar model to simulate chromosomal capture process in early mitosis. Our model conserves the total number of MTs in the cell, reflecting the limited supply of tubulin (37, 38). We find that purely local, decentralized assembly gives the fastest result for hundreds of vesicles, while the combined central/local search is optimal for tens of vesicles (the latter is also relevant for the spindle assembly). The simulations also reveal that unregulated MT branching does not improve the assembly, however, spatially and angularly biased branching accelerates the process. The model suggests that random movements of vesicles or chromosomes and/or rapid inter-MT crosslinking can drastically accelerate the assembly. The simulations result in quantitative estimates that agree with reported experimental measurements.

METHODS

Vesicle Assembly Model

We examine the assembly of vesicles to a central location in the cell through a *search and capture* mechanism mediated by dynamic MTs within a three-dimensional spherical cell, as illustrated in Figure 1 *a*. The system includes a centrally located

centrosome and N_{ves} vesicles, initially randomly dispersed and modeled as small spheres of radius R_{ves}, diffusing within the cell. Both vesicles and centrosome are capable of nucleating MTs. Initially, all vesicles contribute equally to the pool of N_{vMT} vesicle-derived MTs, such that each vesicle grows N_{vMT}/N_{ves} MTs. These MTs, along with N_{cMT} centrosome-derived MTs, are engaged in dynamic instability and explore the cellular space (see Supporting Material for simulation details). When a vesicle is reached by an MT originating from another vesicle, the two instantly merge to a position near either of the original vesicles; the merged vesicle's volume is equal to the sum of the volumes of the pair before the merger. The merged vesicle nucleates a number of MTs equal to the sum of MT numbers nucleated by the merged pair. Newly formed MTs grow in random directions from the merged vesicle. If a vesicle is captured by a centrosomal MT, it is transported toward the cell center instantly and contributes its MTs to the central searcher. MTs that reach the cell boundary undergo immediate depolymerization, resetting their search.

We consider the following scenarios during the vesicle search process:

Unbiased search without branching: MTs explore the cellular space without any bias and branching and with unaltered dynamic instability parameters (growth velocity, v_g, shrinkage velocity, v_s, catastrophe frequency, f_c, and rescue frequency, f_r).

Biased search modulated by a local stabilizing gradient: A spatial bias is introduced by incorporating a stabilizing gradient centered around each vesicle, which influences MT dynamics by modulating the catastrophe frequency. Inspired by the role of RanGTP in chromosomal spindle assembly, this bias is implemented by modeling catastrophe frequency as an exponentially decreasing function of stabilizing agent concentration, which decays with distance from the vesicle (see Eq. S1, Eq. S2, and Supporting Material). This effectively biases MT growth toward nearby vesicles (see Figure 1 *d*). We also explore cases where spontaneous catastrophes are suppressed entirely due to a uniformly distributed global stabilizing agent.

MT branching: MTs can form branches from existing filaments. Each MT is allowed to generate a fixed number (N_{br}) of branch MTs at a rate k_{br}, originating at different distances along the mother MT (see Figure 2 *a*). Secondary branching is excluded. If a branch MT shrinks back to its nucleation site, it dissociates and can re-emerge later from the growing mother MT. Similarly, if the mother MT shrinks past the branch origin, the branch detaches immediately. To conserve the total number of MTs, the nucleation of a branch MT from a central (or local) MT leads to the removal of a randomly chosen MT from the same population. Conversely, when a branch dissociates, a new MT immediately grows from the original source of its mother MT.

Further details of the simulation model are provided in Supporting Material, and parameter values are listed in Table S1.

Chromosomal Capture Model

We simulated the *search and capture* of chromosomes by MTs using an agent-based model (15, 31, 39). The system includes dynamic components – chromosomes, kinetochores, and MTs – and two static centrosomes positioned at opposite poles of a spherical cell. Each centrosome serves as an anchoring site for the minus ends of N_{cMT} centrosomal MTs. Chromosomes are modeled as cylindrical rods with random orientations and are uniformly distributed throughout the cellular volume. Each chromosome contains two sister kinetochores, represented as cylindrical elements positioned back-to-back on the chromosome surface, located at the midpoint along its length. Chromosomes exhibit random motion on the timescale of tens of seconds, undergoing diffusion while maintaining self-avoidance to prevent physical overlap (see Figure S1 *a* and the discussion in the Supporting Material), in contrast to vesicles, which were allowed to approach closely and fuse – consistent with their biological behavior. In addition to translational motion, chromosomes are subject to small rotational displacements at each computational step to represent thermal fluctuations in orientation. A limited degree of rotational diffusion preserves physiological chromosomal dynamics, whereas excessively large rotations can lead to abrupt chromosomal reorientations, resulting in inefficient search in the presence of kinetochore-associated microtubules (ktMTs) (see Figure S1 *b* and discussion in the Supporting Material). N_{ktMT} number of ktMTs emerge from each kinetochore and undergo dynamic instability during the search process. Centrosomal MTs can capture chromosomes either through direct contact with kinetochores or via interaction with ktMTs, with the latter occurring at a rate $k_{inter\text{-}MT}$. Once a kinetochore establishes a connection to a centrosome, by either mechanism, it is considered captured and is no longer available for further capture events. Notably, the translational and rotational motions of a chromosome continue even after one or both kinetochores have been captured (see discussion in the Supporting Material). The *search and capture* process is complete once all kinetochores are successfully attached to spindle MTs.

MTs begin to shrink immediately after contacting the cell boundary or colliding with a chromosome arm (see discussion in the Supporting Material). Upon successful attachment to their target, the captured MTs are replaced by new ones originating from the centrosomes or kinetochores, ensuring that the total number of searcher MTs remains constant throughout the simulation. A schematic representation of the chromosomal assembly process is shown in Figure 5 *a*. Further technical details, including model implementation and parameter values, are provided in Supporting Material and Table S1. As described earlier in the vesicle assembly model, here we also explored three scenarios: (a) MT search with finite catastrophe rates, without bias or branching; (b) inclusion of a RanGTP-like spatial bias, and a comparison with a condition where no spontaneous catastrophes occur inside the cell; and (c) MT

branching from both centrosomal and kinetochore MTs.

To explore the parameter space, we performed 2,000 - 20,000 simulations for each parameter set using different initial configurations. The model was implemented in C and run on an Intel(R) Xeon(R) CPU with a clock speed of 2.20 GHz and 50 GB of RAM. Depending on complexity of the simulated scenario, each simulation took from a few seconds to several minutes. Data analysis and visualization were conducted using GNUPLOT and MATLAB (The MathWorks, Natick, MA).

RESULTS

Coordination among the central and local searching MTs optimizes the vesicle aggregation

We first address the central question: how does the aggregation (assembly) time depend on the MT numbers allocated to the central (centrosomal) and/or local (vesicular) asters if the total MT number is a constant? To find the answer, we examined how the average assembly time varies with the number of MTs emanating from each initial vesicle (Figure 1 *b*). In the simulations, the catastrophe frequency was set so that MTs could grow, on average, up to 1.5 times the cell radius before starting to shorten. Rescue events were suppressed ($f_r = 0$) until microtubules returned to their respective origins, from which they could resume growth in a new random direction (see Supporting Material and Figure S1, *c–f*). Notably, the qualitative trends in assembly time remain robust even when rescue is allowed at a finite rate (Figure S1 *g*).

We found that when the number of vesicles is small (roughly less than 20), allocating all MTs to the central aster, or all MTs to the vesicles, leads to almost the same assembly times, with slightly faster assembly in the central search compared to purely local search (Figure 1, *b* and *c*). The intuitive way to understand this result is based on a simple estimate of the average search time for n targets by an N-MT aster. This time scales as $\sim \ln(n)/N$ (28), because the search time decreases inversely proportionally to the number of searching MTs (two searchers find a target twice faster than one searcher) – this theoretical result agrees with our simulations (compare Figure 1 *c* with Figure S2, *a* and *b*). The logarithmic dependence on the number of targets, apparent from the simulation results (Figure 1 *c*), is due to the fact that the search for n targets is over when all n targets are captured independently. The probability of capturing one target increases with time as $(1 - \exp(-t/\tau))$, where τ is characteristic time of a single capture; the probability of capturing n targets independently is $(1 - \exp(-t/\tau))^n$. After characteristic time of capturing all n targets, T, the probability $(1-\exp(-T/\tau))^n$ is less than 1 by a small number ϵ; as $T > \tau$, $(1 - \exp(-T/\tau))^n \approx 1 - n \cdot \exp(-T/\tau) = 1 - \epsilon$, thus, $T = \tau \ln(n/\epsilon)$. This argument suggests that one central searcher with N MTs captures n vesicles after time $\sim t_0 \ln(n)/N$, where t_0 is a constant parameter. The same argument says that if all MTs are distributed equally between n vesicles, than one of the vesicles captures $(n - 1)$ others after time $\sim t_0 \ln(n - 1)/(N/n)$. As *any* of the vesicles can capture any other one, all vesicles would be assembled after time $\sim (1/n) \cdot t_0 \ln(n - 1)/(N/n) \approx t_0 \ln(n)/N$ – similar to the time of the central assembly. The slight advantage of the central search in this case stems from the geometry: the most distant vesicles from the cell center are one cell radius away, while two most distant vesicles are two radii apart.

The central result of the simulations is that in the case of up to $\sim$ 100 initial vesicles, the average assembly time reaches a minimum at a nontrivial optimal partitioning of MTs between a minority ($\sim 20 - 30\%$) MT number assigned to the centrosome and the rest equally divided between the initial vesicles (Figure 1, *b* and *g*). The time gain is modest but nontrivial and can be understood as follows: initially, some vesicles are much closer to each other than to the cell center, and allowing the vesicles to merge locally accelerates the assembly. At the later stage of the search, when many vesicles are already captured by the centrosome, the number of central MTs becomes the majority, and the last stage of the search is effectively the central one, which is relatively fast for the small number of remaining vesicles. Assigning all MTs to vesicles from the beginning eliminates the central search phase, thereby prolonging assembly.

Another nontrivial result is that for a great number of vesicles, $\gtrsim$ 300, the fastest assembly corresponds to purely local search, and time will only be lost if any MT are assigned to the central search. The explanation is that when the initial vesicle number is great, capturing proximal neighbors is a very fast process, then the merged vesicles with accumulating MT number capture the next neighbors, and so on, with the 'cloud' of vesicles effectively coarsening. This also effectively shifts the vesicles from the cell periphery inward (the peripheral vesicles on average merge inward, toward multiple neighbors in the cell interior. Interior vesicles capture peripheral ones more effectively by searching uniformly in all directions, unlike peripheral vesicles that often search unproductively toward the cell edge), leading to their assembly at an interior position away from the cell center (Figure S2 *c*). Thus, bringing the merged vesicle to the center likely requires at least a few central MTs. Lastly, note that for the great initial vesicle number, the local search is roughly twice faster than the central search (Figure 1 *c*), which is due to smaller, on average, distances between the vesicles capturing each other than between the cell center and vesicles.

We also found that at low vesicle numbers, a very small catastrophe frequency can significantly speed up assembly, even when all MTs are vesicle-nucleated (Figure S2 *d*). At higher catastrophe rates, local MTs from distant vesicles may not persist long enough to reach their targets, while lower catastrophe frequencies enhance MTs persistently grow toward the targets, improving capture efficiency. The simulations also demonstrated that when the vesicles move randomly in the cell, greater effective diffusion coefficient leads to faster as-

sembly (Figure S2 *e*). When the diffusion is faster than certain threshold, differences between various central, local and optimal assembly scenario disappears, because rapid movements bring a vesicle close to the searcher faster than dynamically unstable MTs can capture this vesicle. In what follows, we simulate initial vesicles with a small diffusion constant of the order of $\sim 0.001\ \mu m^2/sec$ (other than during merger events), which keeps MT partitioning strategies relevant for efficient assembly.

Notably, interactions between vesicular MTs and the centrosome were not included in the simulations, due to a lack of direct experimental evidence and the assumption that, without centrosomal MTs, the system represents acentrosomal cells in which vesicles interact only among themselves. To evaluate the effect of such interactions, however, we considered an extended scenario where vesicular MTs can be captured by the centrosome upon contact—even in the absence of centrosomal MTs—resulting in vesicle movement toward the cell center (Figure S2 *f*). This condition shortens assembly times, particularly when most or all MTs are assigned to vesicles, as vesicular MTs then contribute to the central search. Under these circumstances, the previously observed optimal partitioning of MTs for tens of vesicles no longer holds: assigning all MTs to vesicles consistently enhances efficiency, except when the number of vesicles is low ($N_{ves} \lesssim 10$), where a small number of centrosomal MTs still offers an advantage (Figure S2 *g*). Nevertheless, to maintain consistency and biological relevance, we omit these vesicular MT-centrosome interactions from the main analysis.

Spatially biased MT dynamics further accelerates the assembly

Several studies suggest that spatially biased MT growth toward targets enhances search efficiency (28–31). In early mitosis, chromosomes establish a localized biochemical environment that promotes MT nucleation and directional growth. Among the mechanisms responsible, the steep gradient of RanGTP, a RAS-related nuclear protein, centered around chromosomes plays a key role in biasing MT dynamics (23). Within this gradient, MTs tend to grow steadily toward chromosomes while undergoing rapid collapse when growing away. This directional bias can be mimicked by modulating the catastrophe frequency in response to local stabilizing signals (28).

While RanGTP's role is well studied in mitotic chromosome assembly, we investigate whether a similar gradient centered around individual vesicles could bias MTs and reduce the time required for the vesicle assembly. The bias is implemented by reducing the catastrophe frequency near vesicles, modeled as an exponential decay controlled by a stabilizing gradient centered on each vesicle (Figure 1 *d*). Two parameters define the influence of this gradient: the spatial range d_{stab} (how far the stabilizing effect extends from a vesicle), and sensitivity α (how much the catastrophe frequency is decreased by the concentration of the stabilizing agent) (see Eq. S1, Eq. S2, and Supporting Material).

For both central and local searches, biased MT dynamics consistently resulted in faster assembly compared to the unbiased MT dynamics (Figure S2 *h*). The optimized hybrid central/local assembly also showed an improved performance with bias. Moreover, increasing either of the parameters, d_{stab} or α, further shortened the assembly time (Figure 1, *e* and *f*). At large values of both d_{stab} and α, the system approaches a limit where the catastrophe frequency within the cell becomes negligible – similar to an idealized case where MTs never undergo a catastrophe inside the entire cell (Figure 1, *e* and *f*). In this regime, no spontaneous MT catastrophe within the cell occurs, other than when an MT hits the cell boundary. Under such conditions, assigning all MTs to vesicles minimizes the assembly time regardless of the number of the vesicles (Figure S2 *i*). However, when the catastrophe rate is finite, allocating all MTs to the central searcher may become more efficient at low vesicle counts (Figure S2, *d* and *i)*.

Overall, optimal combinations of central and local searchers lead to the fastest assembly in both biased and unbiased scenarios. With very few vesicles, most MTs should be centrally located, while with many vesicles, assigning nearly all MTs to local searchers is optimal (Figure 1 *g*). The lowest assembly times occur when spontaneous catastrophes are absent. Notably, this trend remains consistent even when the total number of MTs is halved or doubled (Figure S2, *a* and *b*). In the following, we simulate MTs without spontaneous catastrophes inside the cell, experiencing catastrophes only at the cell boundary.

Effects of MT branching on the assembly process

As multiple reports indicate that MT branching could play a crucial role in subcellular processes (reviewed in (40)), we explored whether branching from existing MTs could affect vesicle assembly. In the model, the total number of MTs remains constant before and after the branch nucleation (Figure 2 *a*; see also METHODS). In Figure 2 *b*, we compare assembly times with and without MT branching. Each growing central or local searcher MT was allowed to generate up to two branches at a rate of $0.1\ sec^{-1}$, with branches forming at random angles and distances from the mother MT's nucleation site (Figure 2). Note that the literature reports a wide range of branching angles, including values close to 0°, around 20° to 60°, near 90°, and close to 180° (32, 34, 41–44) (also reviewed in (33, 40)). We found that such random branching did not significantly alter the assembly time compared to the no-branching case (Figure 2 *b*).

We next explored whether branching could reduce the assembly time by enhancing MT coverage in peripheral regions of the cell where central MTs splay apart. Two promising strategies would be: (a) initiating branches only after the mother MT grows beyond a certain distance from its origin (defined by the *branching length*, l_{br}), and (b) limiting the

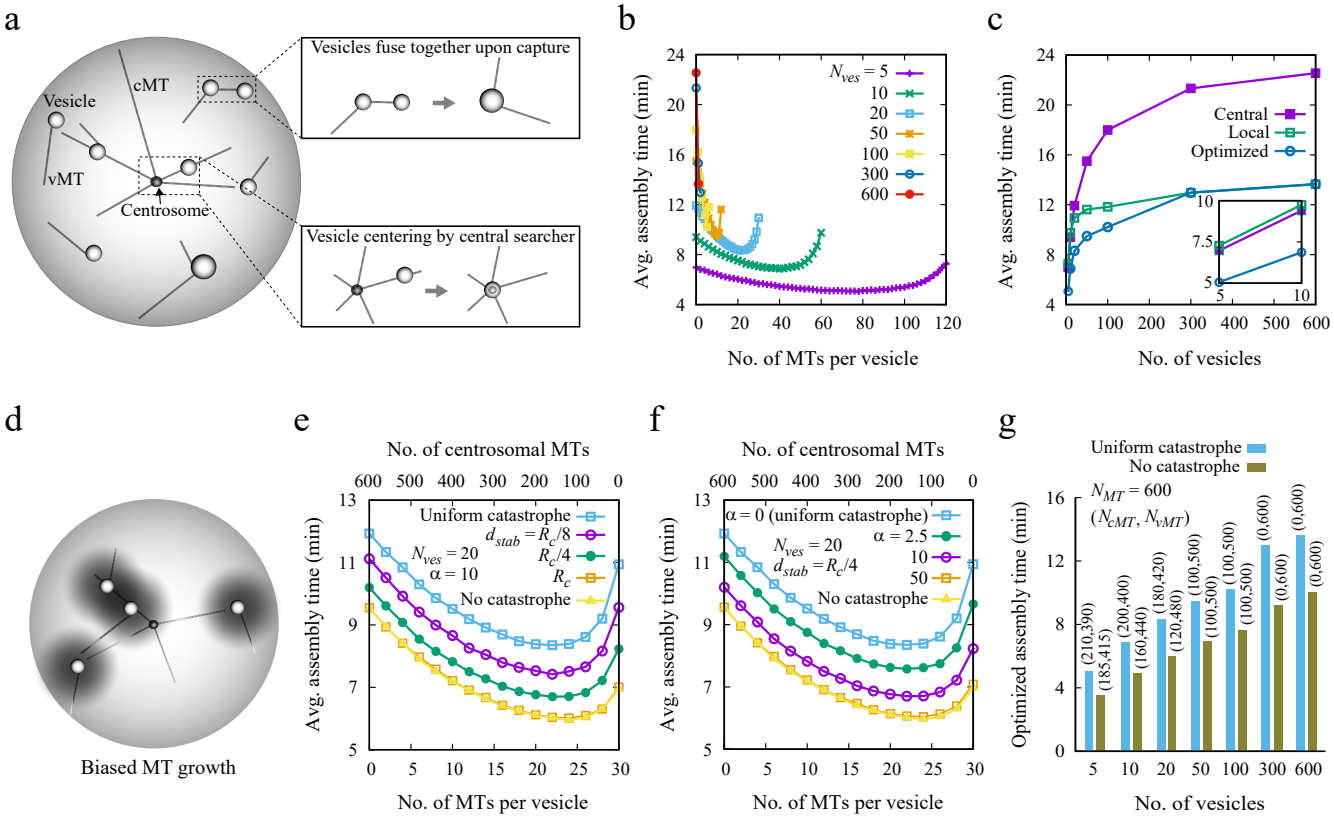

FIGURE 1 Efficient vesicle assembly with distinct MT populations. (*a*) Schematic of the assembly process. Central and local searcher MTs originate from the centrosome and vesicles, respectively. Vesicles merge upon contact via local MTs, conserving volume and MT number (top *inset*). Central searcher MTs guide vesicles toward the center (bottom *inset*). (*b*) Mean assembly time vs. number of MTs per vesicle for N_{ves} = 5, 10, 20, 50, 100, 300, and 600 with uniform catastrophe frequency $f_c = 0.016\,\mathrm{sec}^{-1}$. (*c*) Assembly time vs. vesicle number with MTs assigned only to central or local searchers. The optimal curve combines both MT types, derived from the minima in (*b*). *Inset*: for few vesicles, using only central searcher MTs leads to slightly reduced search times. (*d*) Vesicle assembly with MT bias under stabilizing gradients. Stabilizing agents decay exponentially around vesicles (shaded regions), enhancing MT growth toward targets and effectively destabilizing growth away. (*e–f*) Assembly time vs. MTs per vesicle for N_{ves} = 20 under biased conditions: (*e*) varying d_{stab} at fixed $\alpha = 10$; (*f*) varying α at $d_{\mathrm{stab}} = R_c/4$. Comparisons include unbiased MTs with $f_c = 0.016\,\mathrm{sec}^{-1}$ (uniform catastrophe) and $f_c = 0$ (no spontaneous catastrophe). The top *x*-axis shows corresponding centrosomal MT counts. (*g*) Optimized assembly time vs. vesicle number for both catastrophe scenarios. For 600 total MTs, optimal allocations to centrosomal (N_{cMT}) and vesicular MTs (N_{vMT}) are labeled above bars.

orientation of a branch to a specific angle range relative to the mother MT (the *branch angle*, θ_{br}). To evaluate the impact of these two factors, we plotted the computed average assembly time as a function of parameters l_{br} and θ_{br} for three cases: (i) all MTs originating from the centrosome (N_{cMT} = 600), (ii) all MTs assigned to the vesicles (N_{vMT} = 600), and (iii) an optimized central/local search uncovered in previous non-branching simulations (Figure 3, *a–c*; see also Figure 2 *b*).

Because vesicle-nucleated MTs can grow up to about $2R_c$ in length (for a vesicle located near the cell boundary), while centrosomal MTs' length is limited by the cell radius, we explored a broader range of l_{br} for vesicular MT-based configurations (Figure 3, *b* and *c*) and limited the branching length range to 0–R_c in the central MT-only scenario (Figure 3 *a*). Intermediate values of both l_{br} and θ_{br} produced shorter assembly times than in cases without branching. When central MTs were used, the minimum search time occurred around $l_{br} \approx R_c/2$ (±1.5 µm) and $\theta_{br} \approx 90°$ (±30°) (Figure 3, *a* and *c*). When all MTs were assigned to the vesicles, the optimal region shifted slightly to $l_{br} \approx 2R_c/3$ (±2 µm) and $\theta_{br} \approx 75°$ (±30°) (Figure 3 *b*). The reason for this shift likely stems from the broader spatial distribution of vesicles, allowing vesicular MTs to probe farther regions of the cell compared to central MTs.

These optimal values emerge from a balance between too-

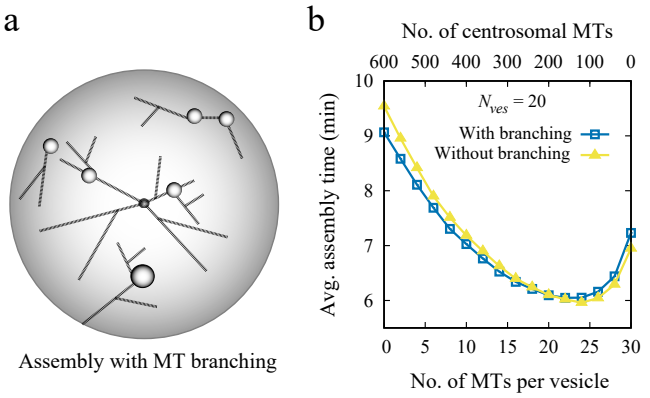

FIGURE 2 Minimal effect of unrestricted MT branching on vesicle assembly time. (*a*) Schematic of MT branching: each MT can produce branches at a given rate, preserving the total number of MTs. Branches form at arbitrary angles and distances along the mother MT. (*b*) Average assembly time vs. number of MTs per vesicle for $N_{ves} = 20$, with and without branching. MTs grow without spontaneous catastrophe ($f_c = 0$). The top x-axis indicates corresponding centrosomal MT counts.

early and too-late branching (Figure 3 *d*). If l_{br} is too small, branching occurs near the MT aster center, spreading MTs too soon and diluting density where it is most needed. Conversely, if branching occurs too late, the mother MTs may have already reached sparse regions, limiting the chances for the branches to capture nearby vesicles. Similarly, extreme values of θ_{br} are suboptimal: large angles effectively return daughter MTs to regions already searched by mother MTs, while MTs branched at small angles search too close to mother MTs (Figure 3 *d*). Intermediate angles allow branches to cover the cell space more effectively, improving the capture of vesicles that might otherwise be missed. Notably, at higher l_{br}, wider θ_{br} values can, in fact, improve efficiency by enabling branches to target gaps between diverging mother MTs (Figure 3, *d* and *e*).

When parameter l_{br} approaches $\sim 0.9R_c$ in the central-only case, the effect of branching becomes negligible, irrespective of θ_{br} values (Figure 3 *a*). Here, mother MTs undergo catastrophe soon after branching, causing branches to disappear before contributing meaningfully and resulting in assembly times similar to the non-branching scenario. In contrast, the vesicle-only system benefits from slightly longer l_{br} and intermediate θ_{br}, likely due to its ability to reach farther into the cell. The hybrid configuration, which includes both central and vesicular MTs for $N_{ves} = 20$, yields an optimal region similar to the central-only case (Figure 3 *c*; see also Figure 3 *a*), but overall assembly time is minimized when all MTs are allocated to the vesicles at higher vesicle counts, especially with $l_{br} \approx R_c/2$ and $\theta_{br} \approx 90^\circ$ (Figure 3 *f*).

Sensitivity of assembly time to the number of branch MTs, rate of branch nucleation, and initial vesicle distribution

To evaluate how sensitive the assembly process is to model parameters, we varied a few parameters at a time while keeping the other parameters fixed at baseline values (Table S1). We first explored how the assembly time depends on the branching length (l_{br}) and branch angle (θ_{br}) for different numbers of MT branches ($N_{br} = 2, 4, 8$) (Figure S3, *a–f*). In both search scenarios (MTs assigned either to the central searcher or to the vesicles), increasing N_{br} expanded the range of l_{br} and θ_{br}, yielding shorter assembly times. More branches increased the chances of reaching the target, either by steering some branches in its direction or by covering more space. For a broader range of l_{br}, additional branches improved spatial coverage (Figure S3 *g*). Even at large values of θ_{br}, some MTs nucleated at favorable angles, maintaining efficiency (Figure S3 *h*). However, at very small values of θ_{br}, the search space narrowed, and adding more branches in that confined region reduced efficiency, increasing assembly time.

We then examined the effect of the branching rate ($k_{br} = 0.1, 0.01, 0.001$ sec^{-1}), assuming that each MT could form two branches (Figure S4). At a high rate of 0.1 sec^{-1}, branches typically nucleated shortly after the mother MT reached l_{br}, yielding optimal l_{br} values around half the cell radius (Figure S4, *a* and *d*). At lower rates, delays in nucleation meant that branching often occurred beyond l_{br}, making those values less effective. Smaller l_{br} values helped initiate earlier branching and improved outcomes at intermediate rates (Figure S4, *b* and *e*). However, at the lowest rate, branching was too infrequent to support efficient search, and assembly times remained high across the full l_{br} range (Figure S4, *c* and *f*).

We also studied how initial vesicle distribution influences the assembly time by restricting the vesicles to a narrow annular region $0.2R_c$ (2 µm) near the cell edge (Figure S5 *a*). Assigning all MTs to vesicles produced assembly time trends similar to that in the case of uniformly distributed vesicles (Figure S5 *b*; see also Figure 3 *b*). In contrast, when all MTs originated from the central searcher, the assembly time increased near $l_{br} \approx 0.8R_c$, just before the vesicle-rich region (Figure S5 *c*). Initiating branches earlier ($l_{br} \approx R_c/2$) or closer to the cell edge ($l_{br} \approx R_c$) improved assembly efficiency, with the shortest assembly time observed for branching near $R_c/2$ (Figure S5, *c* and *d*). This optimal location may seem counterintuitive, as one might expect branching closer to the vesicle-rich zone to more effectively cover the vesicle-populated space. However, with a fixed branch angle, earlier branching (around $R_c/2$) allows branches to explore a broader spatial region, increasing the chance of vesicle encounters. In contrast, late branching near $0.8R_c$ confines the search to a narrow zone around the mother MT, reducing capture efficiency (Figure S5 *d*). While larger branch angles might improve coverage in such cases, branch persistence is limited by the mother MT's stability. When branching occurs near

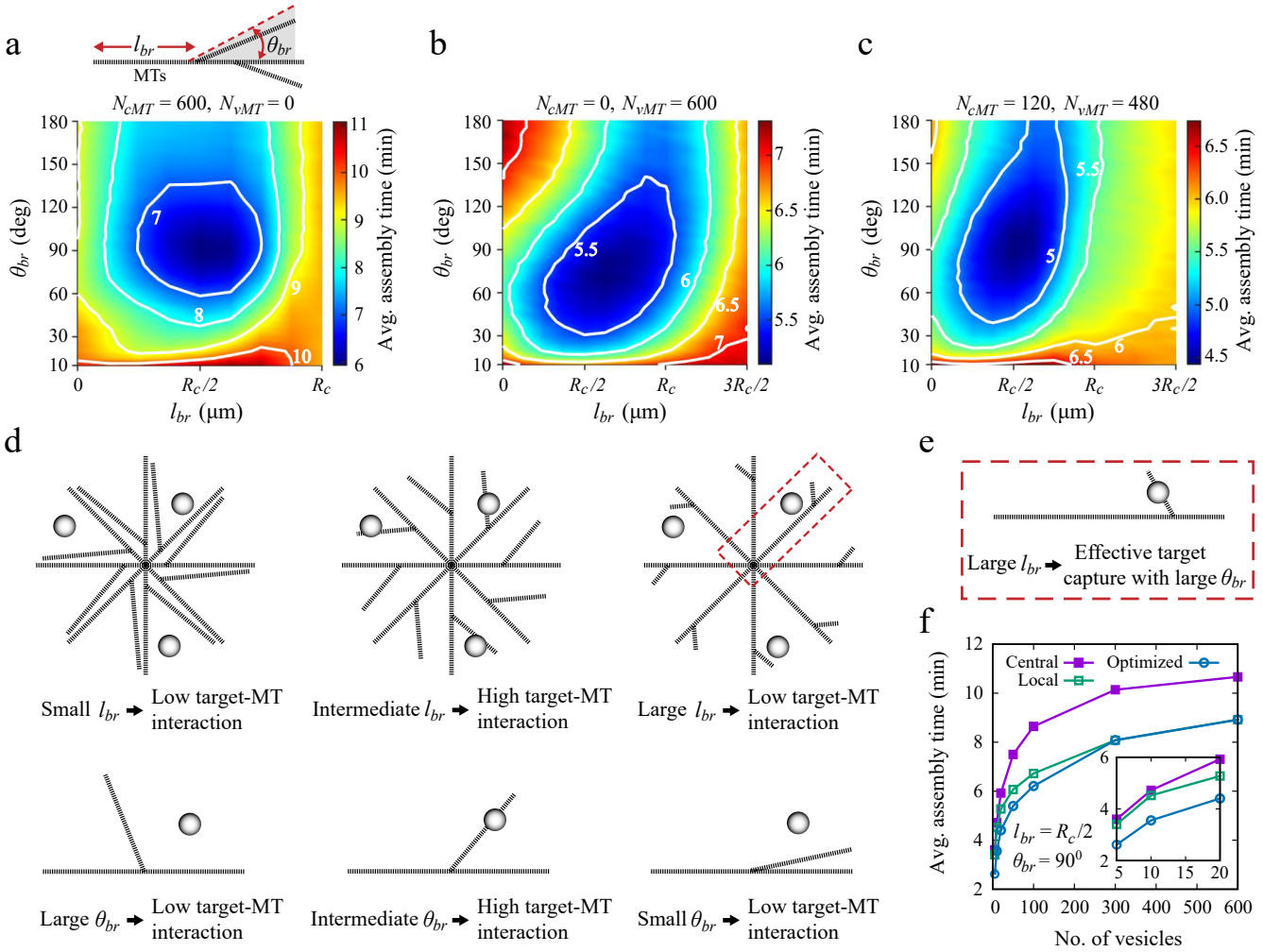

FIGURE 3 Optimizing vesicle assembly with MT branching. (*a*) Average assembly time as a function of branch length (l_{br}) and angle (θ_{br}) for N_{ves} = 20, with all MTs as central searchers (N_{cMT} = 600). (*b*) Same as (*a*), but with all MTs as local searchers (N_{vMT} = 600). (*c*) Assembly time for an optimized mix of central and local searchers (N_{cMT} = 120, N_{vMT} = 480), minimizing time without branching (see Figure 2 *b*). (*d*) Schematic showing how intermediate l_{br} and θ_{br} enhance MT-vesicle contacts. (*e*) At larger l_{br}, wider branching angles improve MT-vesicle targeting compared to narrower ones (see red dotted box in (*d*)). Schematics in (*d*) and (*e*) are simplified representations of the underlying 3D geometry. (*f*) Average assembly time vs. vesicle number for $l_{br} = R_c/2$ and $\theta_{br} = 90°$, comparing central, local, and optimized MT assignments.

$l_{br} \approx 0.8R_c$, close to the cell boundary, the mother MT is more likely to undergo a boundary-induced catastrophe shortly after, causing premature disassembly of its branches as it shrinks past the branch point. Thus, earlier branching (around $R_c/2$) supports a more sustained and spatially extended search, enhancing vesicle capture. Additionally, the shorter assembly time for peripheral branching (near R_c) compared to branching at $0.8R_c$ resulted from the model's rule that forming a new branch removes an existing central MT. As a result, early branching near $l_{br} \approx 0.8R_c$ reduces the number of long MTs that could otherwise reach the vesicles, whereas peripheral branching ($l_{br} \approx R_c$) preserves these long MTs, improving direct targeting (Figure S5 *d*).

We further investigated how the vesicle number influences assembly with the peripheral vesicle distribution. When all MTs were distributed among the vesicles – a configuration favoring optimized assembly time – increasing the number of vesicles slightly increased assembly time, likely due to the broader spatial distribution of the targets. However, when all MTs originated from the central searcher, more vesicles, paradoxically, led to a significant decrease in assembly time (Figure S5 *e*). In this case, once a vesicle near the periphery was captured, it was transported toward the center and became a new site for MT nucleation. This process amplified the central searcher's reach by generating additional MTs, which in turn improved the likelihood of capturing remaining vesicles. Thus,

with more vesicles near the periphery, the feedback between vesicle capture and enhanced MT nucleation at the center accelerated and improved assembly.

Strong inter-MT coupling diminishes the impact of MT branching

So far, we have examined the assembly in which the capture occurs through direct MT–vesicle contact. However, the following scenario is possible: two MTs originating at different vesicles intersect in the cytoplasm, which could lead to MT-MT crosslinking by MT-based molecular motors and/or protein crosslinkers, which indirectly connects the two vesicles together. Then, the motors can, in principle, rapidly bring the vesicles together leading to the merger. There is a relevant example of a similar process in mitotic spindle formation, where centrosomal and kinetochore-derived MTs get interconnected by dynein and NuMA resulting in formation of MT bundles that link kinetochores to the spindle pole (20, 26). Inspired by this example, we examined what happens if we include such crosslinking interactions between MTs from different sources, either central or vesicular, and their branches. We assume in the model that such interactions lead to either vesicle merging or transport to the center, depending on MT origin (Figure 4 *a*). For simplicity, we assumed that upon MT-MT intersection (specifically, when shortest MT-MT distance is less than a threshold equal to MT diameter), the merger of the origins of the MT pair occurs at a single rate $k_{inter-MT}$.

To evaluate the role of this potential process, we varied the number of local searcher MTs per vesicle and measured average assembly times for different interaction rates $k_{inter-MT}$, with and without branching (Figure 4, *b* and *c*). We first fixed the branching angle at $\theta_{br} = 90°$ and varied the branching distance l_{br}, allowing up to two branches per MT to nucleate at a rate of 0.1 sec^{-1}. At low rate $k_{inter-MT}$, the results were similar to those in the non-MT-interacting cases: moderate l_{br} values improved the assembly, while small or large l_{br} slowed it down. As rate $k_{inter-MT}$ increased, differences between the assembly times for different l_{br} values diminished, and at high interaction rates, all conditions converged to similar assembly times, especially when more local MTs were present. Under instantaneous inter-MT capture, the assembly took place super-fast, because hundreds of MTs effectively packed the intracellular space allowing almost instant interactions between the vesicles. In that case, branching offered no added benefit, as vesicle interactions occurred too quickly for branching to influence search efficiency. We also fixed parameter $l_{br} = R_c/2$ and varied parameter θ_{br}. Consistent with earlier results, the assembly was fastest around $\theta_{br} \sim 90°$ at low values of $k_{inter-MT}$, while both smaller and greater angles slowed the process. Again, higher interaction rates reduced these differences, and under instant inter-MT capture, assembly times across all angles became nearly identical to those without branching, making the specific angle of MT branching less critical. Moreover, when MTs frequently interact, interactions among vesicles via local searcher MTs strongly dominate the assembly process over central MT-only configurations, significantly reducing assembly times across vesicle counts (Figure 4 *d*; see also Figure 3 *f*). During spindle assembly, the MT-MT crosslinking seems to take mere tens of seconds (4, 20); thus, based on our simulations, the MT-MT crosslinking with correspondingly high rates can significantly accelerate the assembly.

Chromosome capture during spindle formation is optimized under conditions similar to those of the vesicle assembly

Similar to the vesicle assembly, spindle formation during mitosis relies on two MT populations: centrosomal MTs from two opposite poles and kinetochore MTs from each chromosome (4, 20, 27). Chromosomes can be captured, in principle, either directly via interactions between associated kinetochores and centrosomal MTs, or indirectly through inter-MT interactions between centrosomal and kinetochore MTs at a rate of ~ 0.1 sec^{-1} (4) (Figure 5 *a*).

Our simulations showed, first, that a spatial gradient of MT-stabilizing factors, like RanGTP, around chromosomes, speeds up the search by reducing catastrophe events in MTs growing toward chromosomes (Figure 5, *b–d*). This effect depends on parameter α, which controls the MT dynamic sensitivity to RanGTP, and parameter d_{stab}, the stabilization range (see Eq. S1 and Eq. S2; Supporting Material). Under strong MT stabilization conditions (higher d_{stab} and/or α), average search times approach those in systems without spontaneous MT catastrophes inside the cell (Figure 5, *c* and *d*).

We next examined the potential role of the MT branching in the chromosome capture, if the total MT number is constant. In these simulations, catastrophes occur only upon encountering obstacles such as the cell wall or chromosome arms. MT branches emerge at rate 0.1 sec^{-1} once the mother MT reaches a length l_{br} and within an angle θ_{br} relative to the mother (Figure 5, *insets* in *e* and *f*). Similar to the case of the vesicle assembly, unrestricted branching ($\theta_{br} = 180°, l_{br} = 0$) offers no benefit over the non-branching scenario (Figure 5 *e*). To identify favorable conditions, we varied parameters l_{br} and θ_{br} using the MT arrangement that minimized the search time without branching (Figure 5 *f*; see Figure 5 *e* for the optimized MT combination). Optimal capture is observed when branching occurs at $l_{br} \approx R_c/2$ (± 2.5 µm) and at branch angles $\theta_{br} \approx 30°$ ($\pm 15°$) (Figure 5 *f*). This dynamics likely compensates for the reduced MT density near the spindle poles (conserving total MT number means reducing mother MT number when daughter MTs emerge) by initiating branches farther away from the poles, where mother MTs splay apart. Compared to the vesicle assembly model, the optimal parameter value θ_{br} is lower in the spindle case, likely due to spatial constraints: centrosomal MTs in the spindle assembly are directed inward from the opposite poles, so smaller branching angles help focus growth toward

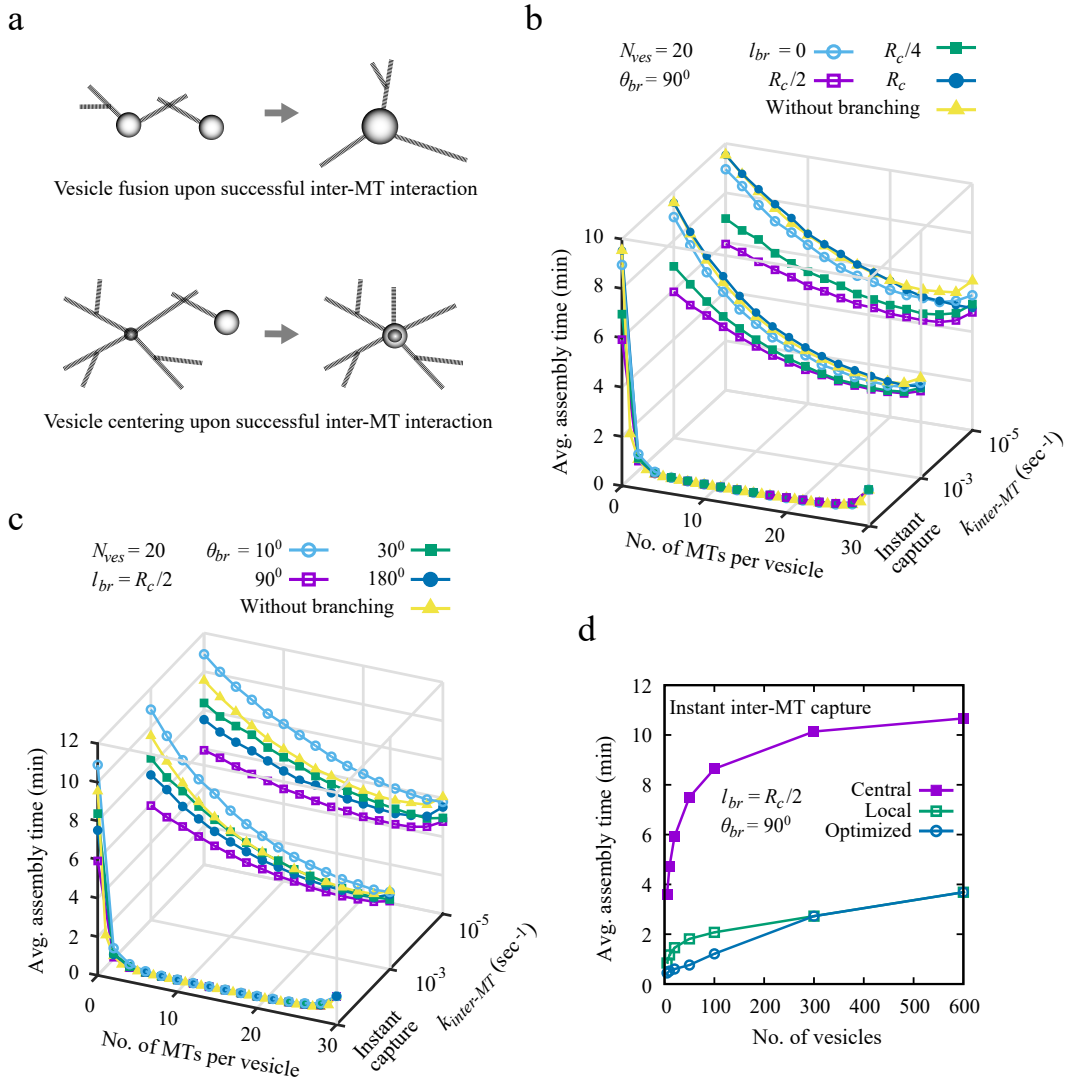

FIGURE 4 Strong inter-MT coupling diminishes branching effects and accelerates assembly, regardless of limited local searchers. (*a*) Schematic showing fusion (merging) of two vesicles (top) and translocation of a vesicle near the centrosome (bottom), following inter-MT coupling. (*b*) Average assembly time vs. MTs per vesicle for $N_{ves} = 20$ at $\theta_{br} = 90°$ and varying branch lengths ($l_{br} = 0, R_c/4, R_c/2, R_c$), for different inter-MT interaction rates: $k_{inter-MT} = 10^{-5}$, 10^{-3} sec^{-1}, and instantaneous capture. (*c*) Assembly time for fixed $l_{br} = R_c/2$ and branch angles $\theta_{br} = 10°, 30°, 90°, 180°$. Results in (*b–c*) are compared with the no-branching case. (*d*) Assembly time vs. vesicle number for $l_{br} = R_c/2$ and $\theta_{br} = 90°$ under instantaneous inter-MT capture, comparing central, local, and optimized MT distributions.

chromosomes. However, excessively small angles delay the spindle assembly.

We next estimate the capture time as a function of the number of kinetochore MTs, allowing instant inter-MT interactions to enable rapid KT capture upon intersection of centrosomal and kinetochore MTs. We compared this scenario to that with a finite MT interaction rate (0.1 sec^{-1}), previously used in Figure 5, *c–f*. With $\theta_{br} = 30°$ and varying l_{br}, finite MT interaction rate shortens search time by branching, but instant capture upon MT-MT interaction yields similar times with or without branching (Figure 5 *g*). Likewise, changing θ_{br} at fixed $l_{br} = R_c/2$ under the instant capture condition has a minimal effect (Figure 5 *h*), suggesting that the MT branching is less important when inter-MT interactions are fast enough.

Finally, we explore how the capture time varies with the number of MTs per kinetochore for different chromosome numbers, considering both finite inter-MT interaction rate ($k_{inter-MT} = 0.1$ sec^{-1}) and instantaneous capture upon intersection of centrosomal and kinetochore MT pair (Figure 5, *i* and *j*). We increase the number of kinetochore MTs while keeping the total MT number fixed, ensuring that each centro-

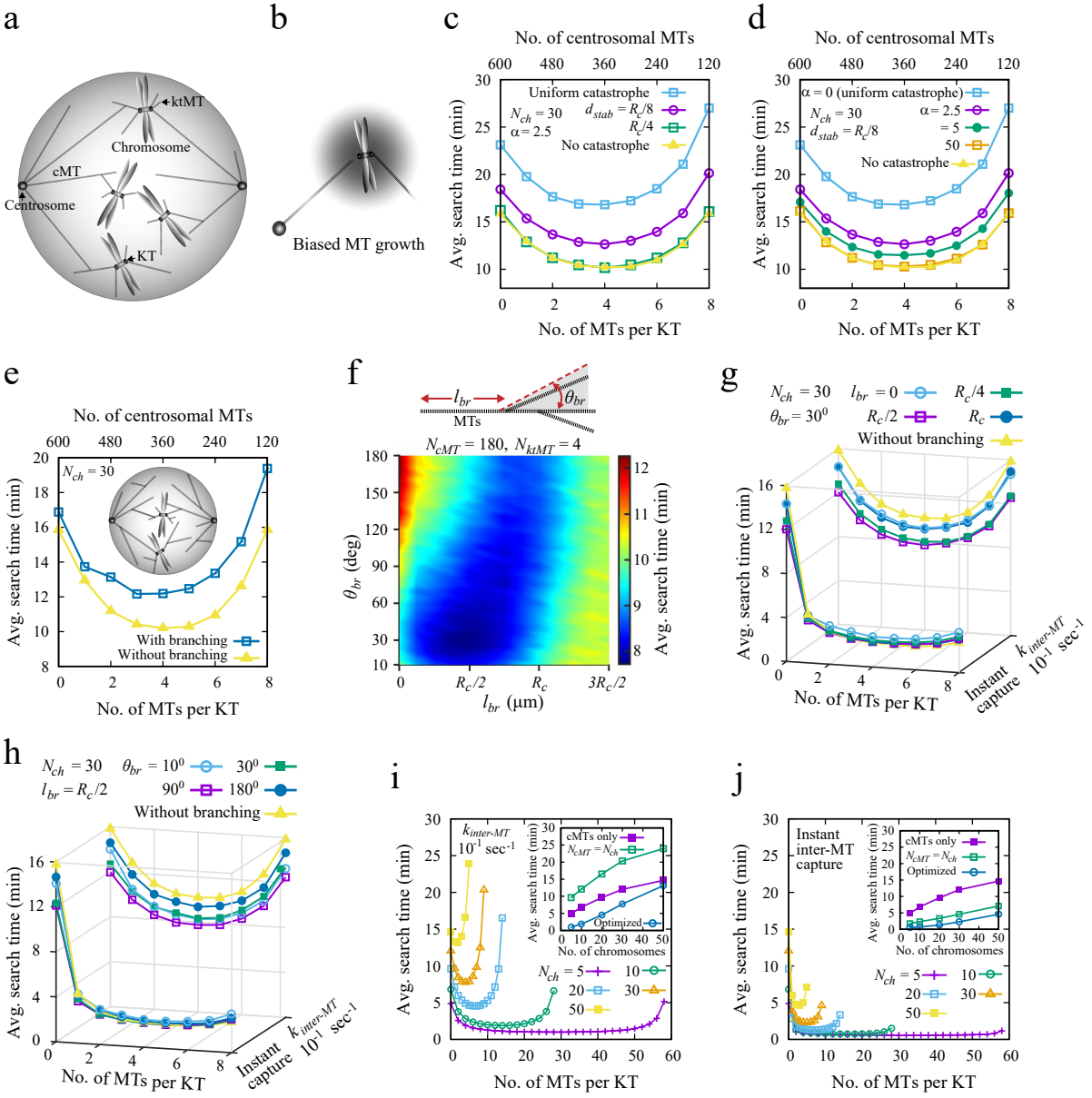

FIGURE 5 Efficient chromosomal capture across MT configurations. (*a*) Schematic of chromosome capture during mitosis, via either centrosomal MTs or associated kinetochore MTs (ktMTs). (*b*) Biased MT growth under a stabilizing RanGTP gradient, which decays exponentially around chromosomes (dark shaded regions), promotes MTs growing toward chromosomes and effectively destabilizes those growing away. (*c–d*) Capture time vs. MTs per KT for biased models with $N_{ch} = 30$ ($N_{kt} = 60$), varying (*c*) d_{stab} ($\alpha = 2.5$) and (*d*) α ($d_{\text{stab}} = R_c/8$). Results are compared with uniform catastrophe ($f_c = 0.016$ sec^{-1}) and no catastrophe inside cell ($f_c = 0$). Top x-axis shows corresponding centrosomal MT numbers. (*e*) Search time vs. MTs per KT with and without branching ($f_c = 0$). *Insets* show MT branching during chromosome search, with branches emerging at variable distances and angles. (*f*) Search time vs. l_{br} and θ_{br} using an optimized MT setup ($N_{cMT} = 180$, $N_{\text{ktMT}} = 4$), based on minimum search time without branching (Figure 5 *e*). (*g–h*) Search time vs. MTs per KT at $k_{inter-MT} = 10^{-1}$ sec^{-1} and with instantaneous MT capture: (*g*) $\theta_{br} = 30°$ and $l_{br} = 0, R_c/4, R_c/2, R_c$; (*h*) $l_{br} = R_c/2$ and $\theta_{br} = 10°, 30°, 90°, 180°$. Both compared to no-branching cases. (*i–j*) Search time vs. MTs per KT for $N_{ch} = 5, 10, 20, 30, 50$ under $k_{inter-MT} = 10^{-1}$ sec^{-1} (*i*) and instantaneous capture (*j*). *Insets* show search time vs. chromosome number with either centrosome-only MTs (300 cMTs per centrosome) or minimal MT allocation across centrosomes ($N_{cMT} = N_{ch}$). Optimal search times are taken from the minima in (*i*) and (*j*).

some has at least N_{ch} centrosomal MTs for a system with N_{ch} chromosomes. Since each chromosome has two kinetochores, at least N_{ch} centrosomal MTs per pole are needed to connect all chromosomes to the spindle. We observe that the search time reaches a minimum at certain optimal number of kinetochore MTs (Figure 5 *i*). However, when centrosomal MTs are limited to $N_{cMT} = N_{ch}$, assembly is slower compared to a configuration where all MTs are centrosomal (Figure 5 *i*, *inset*). In this case, the lower availability of centrosomal MTs, combined with finite inter-MT interactions, delays chromosome capture. By contrast, under instantaneous inter-MT interaction, kinetochore MTs significantly improve efficiency for any chromosome number, even when centrosomal MTs are scarce (Figure 5 *j*; see also *inset*).

DISCUSSION AND CONCLUSIONS

The main conclusion of our study, as summarized in Figure 6, is that when MT pool is limited, there is an optimal combination of central (centrosome-anchored) and local (vesicle-anchored) MTs for the fastest assembly of tens of Golgi vesicles or pigment particles at the cell center. The optimal MT partitioning corresponds to a minor fraction of MTs (on the order of 20 to 30%) assigned initially to the centrosome, while the majority of the MTs should be equipartitioned between the vesicles. As the assembly proceeds, the centralized MT number will grow. The qualitative explanation for these predictions is that the local assembly far away from the cell center is much more effective than the centralized search by splayed-out MTs near the cell periphery, while the central search of few aggregates at the last stage accelerates the final assembly. The model predicts that in the characteristic mitotic spindles with tens of chromosomes, the fastest integration of all these chromosomes into the bipolar spindle occurs when roughly half (a few hundreds) of MTs emanate from two spindle poles, while the remainder – comprising several MTs per kinetochore – are associated with the chromosomes. These estimates semi-quantitatively (experimental measurements of MT numbers in live cells remain elusive) agree with observations of Golgi reassembly (10), pigment granules' aggregations in melanophores (3, 11) and spindle assembly (20, 27).

Notably, the predicted acceleration in the optimal regime is relatively modest compared to purely local or centralized searches – just a few minutes faster – but at least in the spindle assembly case, every one of the gained minutes could be important (45). The model correctly estimates that Golgi vesicles can be reassembled in 10-20 minutes (10), while the spindle can be assembled in a few minutes (4, 27).

Interestingly, the model prediction for hundreds of vesicles or granules is that purely local search is the fastest - the local assembly of many proximal vesicles proves highly efficient and enables rapid assembly even in the absence of a centrosome. Indeed, Golgi-derived MTs can assemble the Golgi complex from dispersed ministacks without centrosomes (46), while melanosome aggregation in fish melanophores, can proceed via local MTs alone (11). The caveat of this prediction, however, is that the simulated vesicles may cluster away from the cell center, suggesting that a very few central MTs are likely required to gather the last few vesicle clumps to the centrosome. This supports the findings of Vinogradova et al. (10), who suggested that centrosomal MT asters play an important role in Golgi organization, thereby rendering the central search essential.

The model suggests that the assembly is most effective in the absence of MT catastrophes inside the cell, away from the cell boundary. For finite catastrophe rates, shifting more MTs to local searches improves the outcome in general, while the optimal MT partitioning between the central and local searchers outlined in the previous paragraphs still holds. For finite catastrophe rates, the model predicts that a gradient of stabilizing agents around vesicles can accelerate the assembly. Similar prediction is made in the spindle assembly model, which aligns with theoretical (28, 31) and experimental findings (29, 30). We also examine the regime in which strong, long-range stabilization by multiple chromosomes suppresses spontaneous catastrophes throughout the cell, effectively creating a uniformly stabilizing environment. This is consistent with the findings of Athale et al. (29), who demonstrated that only long-range, steeply decaying gradients could account for the observed MT aster organization around chromosomes in their experiments. In our model, such overlapping gradients from several chromosomes reduce assembly time by promoting MT growth throughout the cell interior.

Our results show that unbiased MT branching does not improve the assembly, however, biased branching that occurs after the mother MT has grown to approximately half the cell radius, and when branches form at specific angles, around $90°(\pm 30°)$ for vesicle assembly and $30°(\pm 15°)$ for chromosome capture, significantly accelerates the assembly. The difference in the two optimal angles is due to the searching the entire cell volume during the vesicle assembly process, compared to a searching a smaller volume around the cell equator from the poles in the spindle assembly process. These findings are consistent with experimental observations of shallow-angled MT branching in mitotic/meiotic spindles (32–34) — where branches form mostly along the middle of the mother microtubule (32) — and in interphase plant cells (33, 41, 43), suggesting that cells regulate branch initiation position and angle to maintain high MT density at the periphery (47). Additionally, our model includes only primary branches nucleating from the mother microtubule and excludes secondary branching from existing branches. Such higher-order branching could introduce additional hierarchies, with some branches potentially pointing back toward the origin (e.g., the centrosome or vesicles/kinetochores), thereby reducing search efficiency. This effect is partially captured in our analysis of large branch angles, which can hinder efficiency by allowing near-antiparallel branch nucleation relative to the mother MT. A full investigation of higher-order

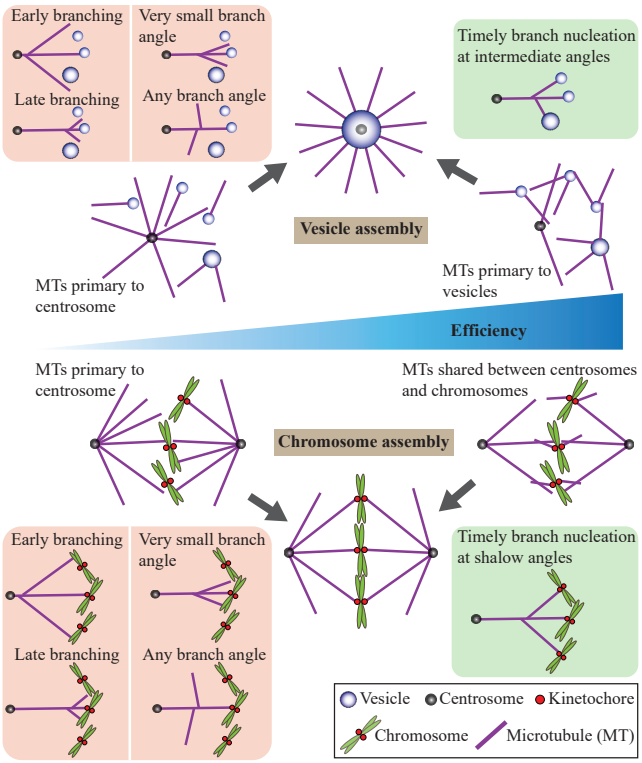

FIGURE 6 Summary of key outcomes showing efficient vesicle and chromosome assembly under different MT arrangements. Compared to cases where most MTs originate from centrosomes, assigning MTs primarily to vesicles or sharing them between centrosomes and chromosomes results in more efficient assembly. MT branches that nucleate either too early or too late, or at very narrow or wide angles, reduce search efficiency. In contrast, timely branching at intermediate distances and angles improves overall assembly efficiency. Strong coupling between MTs from different origins reduces the effect of branching and drastically accelerates assembly efficiency (not shown here; see Figure 4 and Figure 5, *g–j*).

branching, however, lies beyond the present scope.

If vesicles or chromosomes are engaged in rapid enough random movements during the assembly processes, the assembly duration decreases and MT partitioning strategy is irrelevant, because these movements bring a vesicle or a chromosome close enough to a searcher fast enough. The simulations show that an effective diffusion coefficient of the order of 0.001 μm^2/sec is the threshold between the two regimes. Thermal diffusion of a 0.1 µm-radius vesicles in cytoplasm with viscosity 1000 times higher than that of water, according to Stockes' formula, is on the order of 0.001 μm^2/sec (48), so our simulations of the assembly of low-mobility vesicles, which are larger than 0.1 µm in radius and of ~ 1 µm-large chromosomes are relevant.

Spindle assembly proceeds in the presence of crosslinking of MT pairs originating from the spindle poles (centrosomes) and the kinetochores, mediated by proteins such as dynein and NuMA (20, 26). In the spindle, such inter-MT crosslinking can occur within tens of seconds (20). The model demonstrates that MT crosslinking that is so fast can drastically accelerate the spindle assembly; similar result is valid for the vesicle assembly. The explanation is that in the presence of the fast crosslinking MTs essentially search for each other, rather than solely targeting vesicles, and it could be much faster to interconnect two vesicles by intersecting MTs than to find the vesicle by a MT. Interestingly, the model predicts that rapid crosslinking makes purely central search worse than the local assembly for any number of vesicles.

Several factors, in addition to more complex cell geometry, may require refining our model. It remains to be tested whether cells maintain a constant total MT number. Assembly of Golgi complex involves more complexity than simply bringing the vesicles together: only the trans side of the Golgi supports MT tethering (49), and MT nucleation may be restricted to specific vesicle regions (49, 50). Similarly, chromosome orientation (31), kinetochore architecture (39) and initial geometry of chromosomes' distribution across the cell (51), and chromosome size distribution (52) affect the spindle assembly making it much more complex and nuanced than in our model here. MT pivoting, which we did not consider, could further accelerate the assembly (53, 54). There are additional MT networks in some cells, i.e. those anchored on the nuclear envelope in myotubes (55) and the apical membrane in polarized epithelial cells (56), which are not accounted for in the model. Moreover, our model is purely geometric and does not account for mechanics of intracellular movements (15, 57, 58). Last, but not least, the model does not yet include error correction mechanisms that are likely to prolong the correct assembly (59–61).

AUTHOR CONTRIBUTIONS

R.P., A.M., and A.S. conceived the study and wrote the paper together. R.P. and A.S. developed the numerical code and ran the simulations.

DECLARATION OF INTERESTS

The authors declare no competing interests.

ACKNOWLEDGMENTS

R.P. and A.S. thank Indian Association for the Cultivation of Science (IACS) for funding and computational facilities. A.M. acknowledges the support from National Science Foundation (Grant no. DMS1953430).

SUPPORTING CITATIONS

References (62–74) appear in the Supporting Material.

REFERENCES

1. Westermann, B., 2010. Mitochondrial fusion and fission in cell life and death. *Nat. Rev. Mol. Cell Biol.* 11:872–884.

2. Gaietta, G. M., B. N. G. Giepmans, T. J. Deerinck, W. B. Smith, L. Ngan, J. Llopis, S. R. Adams, R. Y. Tsien, and M. H. Ellisman, 2006. Golgi twins in late mitosis revealed by genetically encoded tags for live cell imaging and correlated electron microscopy. *Proc. Natl. Acad. Sci. USA.* 103:17777–17782.

3. Lomakin, A. J., P. Kraikivski, I. Semenova, K. Ikeda, I. Zaliapin, J. S. Tirnauer, A. Akhmanova, and V. Rodionov, 2011. Stimulation of the CLIP-170–dependent capture of membrane organelles by microtubules through fine tuning of microtubule assembly dynamics. *Mol. Biol. Cell.* 22:4029–4037.

4. Renda, F., C. Miles, I. Tikhonenko, R. Fisher, L. Carlini, T. M. Kapoor, A. Mogilner, and A. Khodjakov, 2022. Non-centrosomal microtubules at kinetochores promote rapid chromosome biorientation during mitosis in human cells. *Curr. Biol.* 32:1049–1063.

5. Warren, G., and W. Wickner, 1996. Organelle Inheritance. *Cell.* 84:395–400.

6. Colanzi, A., C. Suetterlin, and V. Malhotra, 2003. Cell-cycle-specific Golgi fragmentation: how and why? *Curr. Opin. Cell Biol.* 15:462–467.

7. Colanzi, A., C. Sutterlin, and V. Malhotra, 2003. RAF1-activated MEK1 is found on the Golgi apparatus in late prophase and is required for Golgi complex fragmentation in mitosis. *J. Cell Biol.* 161:27–32.

8. Alberts, B., A. Johnson, J. Lewis, M. Raff, K. Roberts, and P. Walter, 2002. Molecular biology of the cell. New York: Garland Science.

9. Kirschner, M., and T. Mitchison, 1986. Beyond self-assembly: From microtubules to morphogenesis. *Cell.* 45:329–342.

10. Vinogradova, T., R. Paul, A. D. Grimaldi, J. Lončarek, P. M. Miller, D. Yampolsky, V. Magidson, A. Khodjakov, A. Mogilner, and I. Kaverina, 2012. Concerted effort of centrosomal and Golgi-derived microtubules is required for proper Golgi complex assembly but not for maintenance. *Mol. Biol. Cell.* 23:820–833.

11. Malikov, V., E. N. Cytrynbaum, A. Kashina, A. Mogilner, and V. Rodionov, 2005. Centering of a radial microtubule array by translocation along microtubules spontaneously nucleated in the cytoplasm. *Nat. Cell Biol.* 7:1213–1218.

12. Tolić-Nørrelykke, I. M., 2008. Push-me-pull-you: how microtubules organize the cell interior. *Eur. Biophys. J.* 37:1271–1278.

13. Pavin, N., and I. M. Tolić-Nørrelykke, 2014. Swinging a sword: how microtubules search for their targets. *Syst. Synth. Biol.* 8:1103.

14. de Saint Phalle, B., and W. Sullivan, 1998. Spindle Assembly and Mitosis without Centrosomes in Parthenogenetic Sciara Embryos. *J. Cell Biol.* 141:1383–1391.

15. Heald, R., and A. Khodjakov, 2015. Thirty years of search and capture: The complex simplicity of mitotic spindle assembly. *J. Cell Biol.* 211:1103.

16. Chabin-Brion, K., J. Marceiller, F. Perez, C. Settegrana, A. Drechou, G. Durand, and C. Poüs, 2001. The Golgi complex is a microtubule-organizing organelle. *Mol. Biol. Cell.* 12:2047–2060.

17. Maiato, H., C. L. Rieder, and A. Khodjakov, 2004. Kinetochore-driven formation of kinetochore fibers contributes to spindle assembly during animal mitosis. *J. Cell Biol.* 167:831–840.

18. Kitamura, E., K. Tanaka, S. Komoto, Y. Kitamura, C. Antony, and T. U. Tanaka, 2010. Kinetochores Generate Microtubules with Distal Plus Ends: Their Roles and Limited Lifetime in Mitosis. *Dev. Cell.* 18:248–259.

19. Karsenti, E., J. Newport, and M. Kirschner, 1984. Respective roles of centrosomes and chromatin in the conversion of microtubule arrays from interphase to metaphase. *J. Cell Biol.* 99:47s–54s.

20. Sikirzhytski, V., V. Magidson, J. B. Steinman, J. He, M. L. Berre, I. Tikhonenko, J. G. Ault, B. F. McEwen, J. K. Chen, H. Sui, M. Piel, T. M. Kapoor, and A. Khodjakov, 2014. Direct kinetochore–spindle pole connections are not required for chromosome segregation. *J. Cell Biol.* 206:231–243.

21. Miller, P. M., A. W. Folkmann, A. R. R. Maia, N. Efimova, A. Efimov, and I. Kaverina, 2009. Golgi-derived CLASP-dependent microtubules control Golgi organization and polarized trafficking in motile cells. *Nat. Cell. Biol.* 11:1069–80.

22. Semenova, I., D. Gupta, T. Usui, I. Hayakawa, A. Cowan, and V. Rodionov, 2017. Stimulation of microtubule-based transport by nucleation of microtubules on pigment granules. *Mol. Biol. Cell.* 28:1418–1425.

23. Prosser, S. L., and L. Pelletier, 2017. Mitotic spindle assembly in animal cells: a fine balancing act. *Nat. Rev. Mol. Cell Biol.* 18:187–201.

24. Valdez, V. A., L. Neahring, S. Petry, and S. Dumont, 2023. Mechanisms underlying spindle assembly and robustness. *Nat. Rev. Mol. Cell Biol.* 24:523–542.

25. Goshima, G., F. Nédélec, and R. D. Vale, 2005. Mechanisms for focusing mitotic spindle poles by minus end-directed motor proteins. *J. Cell Biol.* 171:229–240.

26. Elting, M. W., C. L. Hueschen, D. B. Udy, and S. Dumont, 2014. Force on spindle microtubule minus ends moves chromosomes. *J. Cell Biol.* 206:245–256.

27. Sikirzhytski, V., F. Renda, I. Tikhonenko, V. Magidson, B. F. McEwen, and A. Khodjakov, 2018. Microtubules assemble near most kinetochores during early prometaphase in human cells. *J. Cell Biol.* 217:2647–2659.

28. Wollman, R., E. Cytrynbaum, J. Jones, T. Meyer, J. Scholey, and A. Mogilner, 2005. Efficient chromosome capture requires a bias in the 'search-and-capture' process during mitotic spindle assembly. *Curr. Biol.* 15:828–832.

29. Athale, C. A., A. Dinarina, M. Mora-Coral, C. Pugieux, F. Nedelec, and E. Karsenti, 2008. Regulation of microtubule dynamics by reaction cascades around chromosomes. *Science.* 322:1243–1247.

30. Carazo-Salas, R. E., G. Guarguaglini, O. J. Gruss, A. Segref, E. Karsenti, and I. W. Mattaj, 1999. Generation of GTP-bound Ran by RCC1 is required for chromatin-induced mitotic spindle formation. *Nature.* 400:178–181.

31. Paul, R., R. Wollman, W. T. Silkworth, I. K. Nardi, D. Cimini, and A. Mogilner, 2009. Computer simulations predict that chromosome movements and rotations accelerate mitotic spindle assembly without compromising accuracy. *Proc. Natl. Acad. Sci. USA.* 106:15708–15713.

32. Petry, S., A. C. Groen, K. Ishihara, T. J. Mitchison, and R. D. Vale, 2013. Branching microtubule nucleation in Xenopus egg extracts mediated by augmin and TPX2. *Cell.* 152:768–777.

33. Sánchez-Huertas, C., and J. Lüders, 2015. The Augmin Connection in the Geometry of Microtubule Networks. *Curr. Biol.* 25:R294–R299.

34. Kamasakim, T., E. O'Toole, S. Kita, M. Osumi, J. Usukura, J. R. McIntosh, and G. Goshima, 2013. Augmin-dependent microtubule nucleation at microtubule walls in the spindle. *J. Cell Biol.* 202:25–33.

35. Decker, F., D. Oriola, B. Dalton, and J. Brugués, 2018. Autocatalytic microtubule nucleation determines the size and mass of Xenopus laevis egg extract spindles. *Elife.* 7:e31149.

36. Gouveia, B., S. U. Setru, M. R. King, A. Hamlin, H. A. Stone, J. W. Shaevitz, and S. Petry, 2023. Acentrosomal spindles assemble from branching microtubule nucleation near chromosomes in Xenopus laevis egg extract. *Nat. Commun.* 14:3696.

37. Tulu, U. S., C. Fagerstrom, N. P. Ferenz, and P. Wadsworth, 2006. Molecular Requirements for Kinetochore-Associated Microtubule Formation in Mammalian Cells. *Curr. Biol.* 16:536–541.

38. Hayward, D., J. Metz, C. Pellacani, and J. G. Wakefield, 2014. Synergy between Multiple Microtubule-Generating Pathways Confers Robustness to Centrosome-Driven Mitotic Spindle Formation. *Dev. Cell.* 28:81–93.

39. Magidson, V., R. Paul, N. Yang, J. G. Ault, C. B. O'Connell, I. Tikhonenko, B. F. McEwen, A. Mogilner, and A. Khodjakov, 2015. Adaptive changes in the kinetochore architecture facilitate proper spindle assembly. *Nat. Cell Biol.* 17:1134–1144.

40. Travis, S. M., B. P. Mahon, and S. Petry, 2022. How Microtubules Build the Spindle Branch by Branch. *Annu. Rev. Cell Dev. Biol.* 38:1–23.

41. Murata, T., S. Sonobe, T. I. Baskin, S. Hyodo, S. Hasezawa, T. Nagata, T. Horio, and M. Hasebe, 2005. Microtubule-dependent microtubule nucleation based on recruitment of γ-tubulin in higher plants. *Nat. Cell Biol.* 7:961–968.

42. Verma, V., and T. J. Maresca, 2019. Direct observation of branching MT nucleation in living animal cells. *J. Cell Biol.* 218:2829–2840.

43. Chan, J., A. Sambade, G. Calder, and C. Lloyd, 2009. Arabidopsis cortical microtubules are initiated along, as well as branching from, existing microtubules. *Plant Cell.* 21:2298–2306.

44. Janson, M. E., T. G. Setty, A. Paoletti, and P. Tran, 2005. Efficient formation of bipolar microtubule bundles requires microtubule-bound γ-tubulin complexes. *J. Cell Biol.* 169:297–308.

45. Heald, R., R. Tournebize, T. Blank, R. Sandaltzopoulos, P. Becker, A. Hyman, and E. Karsenti, 1996. Self-organization of microtubules into bipolar spindles around artificial chromosomes in Xenopus egg extracts. *Nature.* 382:420–425.

46. Tängemo, C., P. Ronchi, J. Colombelli, U. Haselmann, J. C. Simpson, C. Antony, E. H. K. Stelzer, R. Pepperkok, and E. G. Reynaud, 2011. A novel laser nanosurgery approach supports de novo Golgi biogenesis in mammalian cells. *J. Cell Sci.* 124:978–987.

47. Ishihara, K., K. S. Korolev, and T. J. Mitchison, 2016. Physical basis of large microtubule aster growth. *Elife*. 5:e19145.

48. Mogilner, A., and A. Manhart, 2018. Intracellular Fluid Mechanics: Coupling Cytoplasmic Flow with Active Cytoskeletal Gel. *Annu. Rev. Fluid Mech.* 50:347–370.

49. Efimov, A., A. Kharitonov, N. Efimova, J. Loncarek, P. M. Miller, N. Andreyeva, P. Gleeson, N. Galjart, A. R. Maia, I. X. McLeod, et al., 2007. Asymmetric CLASP-dependent nucleation of noncentrosomal microtubules at the trans-Golgi network. *Dev. Cell.* 12:917–930.

50. Rivero, S., J. Cardenas, M. Bornens, and R. M. Rios, 2009. Microtubule nucleation at the cis-side of the Golgi apparatus requires AKAP450 and GM130. *EMBO J.* 28:1016–28.

51. Magidson, V., C. B. O'Connell, J. Lončarek, R. Paul, A. Mogilner, and A. Khodjakov, 2011. The Spatial Arrangement of Chromosomes during Prometaphase Facilitates Spindle Assembly. *Cell.* 146:555–567.

52. Nayak, P., S. Chatterjee, and R. Paul, 2023. Microtubule search-and-capture model evaluates the effect of chromosomal volume conservation on spindle assembly during mitosis. *Phys. Rev. E.* 108:034401.

53. Kalinina, I., A. Nandi, P. Delivani, M. R. Chacón, A. H. Klemm, D. Ramunno-Johnson, A. Krull, B. Lindner, N. Pavin, and I. M. Tolić-Nørrelykke, 2013. Pivoting of microtubules around the spindle pole accelerates kinetochore capture. *Nat. Cell Biol.* 15:82–87.

54. Blackwell, R., O. Sweezy-Schindler, C. Edelmaier, Z. R. Gergely, P. J. Flynn, S. Montes, A. Crapo, A. Doostan, R. McIntosh, M. A. Glaser, and M. D. Betterton, 2017. Contributions of Microtubule Dynamic Instability and Rotational Diffusion to Kinetochore Capture. *Biophys. J.* 112:552–563.

55. Tassin, A. M., B. Maro, and M. Bornens, 1985. Fate of microtubule-organizing centers during myogenesis in vitro. *J. Cell Biol.* 100:35–46.

56. Feldman, J. L., and J. R. Priess, 2012. A Role for the Centrosome and PAR-3 in the Hand-Off of MTOC Function during Epithelial Polarization. *Curr. Biol.* 22:575–582.

57. Corthésy-Theulaz, I., A. Pauloin, and S. R. Pfeffer, 1992. Cytoplasmic dynein participates in the centrosomal localization of the Golgi complex. *J. Cell Biol.* 118:1333–1345.

58. Mogilner, A., R. Wollman, G. Civelekoglu-Scholey, and J. Scholey, 2006. Modeling mitosis. *Trends Cell Biol.* 16:88–96.

59. Ault, J. G., and C. L. Rieder, 1992. Chromosome malorientation and reorientation during mitosis. *Cell Motil. Cytoskeleton.* 22:155–159.

60. Lampson, M. A., and E. L. Grishchuk, 2017. Mechanisms to avoid and correct erroneous kinetochore-microtubule attachments. *Biology.* 6:1.

61. Lakshmi, R. B., P. Nayak, L. Raz, A. Sarkar, A. Saroha, P. Kumari, V. M. Nair, D. P. Kombarakkaran, S. Sajana, S. MG, et al., 2024. CKAP5 stabilizes CENP-E at kinetochores by regulating microtubule-chromosome attachments. *EMBO Rep.* 25:1909–1935.

62. Rusan, N. M., C. J. Fagerstrom, A.-M. C. Yvon, and P. Wadsworth, 2001. Cell Cycle-Dependent Changes in Microtubule Dynamics in Living Cells Expressing Green Fluorescent Protein-α Tubulin. *Mol. Biol. Cell.* 12:971–980.

63. Holy, T., and S. Leibler, 1994. Dynamic instability of microtubules as an efficient way to search in space. *Proc. Natl. Acad. Sci. USA.* 91:5682–5685.

64. Sarkar, A., R. Paul, and H. Rieger, 2019. Search and Capture Efficiency of Dynamic Microtubules for Centrosome Relocation during IS Formation. *Biophys. J.* 116:2079–2091.

65. Gopalakrishnan, M., and B. S. Govindan, 2011. A first-passage-time theory for search and capture of chromosomes by microtubules in mitosis. *Bull. Math. Biol.* 73:2483–2506.

66. Janson, M. E., M. E. de Dood, and M. Dogterom, 2003. Dynamic instability of microtubules is regulated by force. *J. Cell Biol.* 161:1029–1034.

67. Tran, P., L. Marsh, V. Doye, S. Inoue, and F. Chang, 2001. A mechanism for nuclear positioning in fission yeast based on microtubule pushing. *J. Cell Biol.* 153:397–412.

68. Kozlowski, C., M. Srayko, and F. Nedelec, 2007. Cortical microtubule contacts position the spindle in C. elegans embryos. *Cell.* 129:499–510.

69. Tischer, C., D. Brunner, and M. Dogterom, 2009. Force- and kinesin-8-dependent effects in the spatial regulation of fission yeast microtubule dynamics. *Mol. Syst. Biol.* 5:250.

70. Dogterom, M., J. W. Kerssemakers, G. Romet-Lemonne, and M. E. Janson, 2005. Force generation by dynamic microtubules. *Curr. Opin. Cell Biol.* 17:67–74.

71. Brouhard, G. J., and A. J. Hunt, 2005. Microtubule movements on the arms of mitotic chromosomes: polar ejection forces quantified in vitro. *Proc. Natl. Acad. Sci. USA.* 102:13903–13908.

72. Vorozhko, V. V., M. J. Emanuele, M. J. Kallio, P. T. Stukenberg, and G. J. Gorbsky, 2008. Multiple mechanisms of chromosome movement in vertebrate cells mediated through the Ndc80 complex and dynein/dynactin. *Chromosoma.* 117:169–179.

73. Wood, K. W., R. Sakowicz, L. S. Goldstein, and D. W. Cleveland, 1997. CENP-E is a plus end–directed kinetochore motor required for metaphase chromosome alignment. *Cell.* 91:357–366.

74. Mazumdar, M., and T. Misteli, 2005. Chromokinesins: multitalented players in mitosis. *Trends Cell Biol.* 15:349–355.

Supplemental Information

Supplemental Figures and Legends

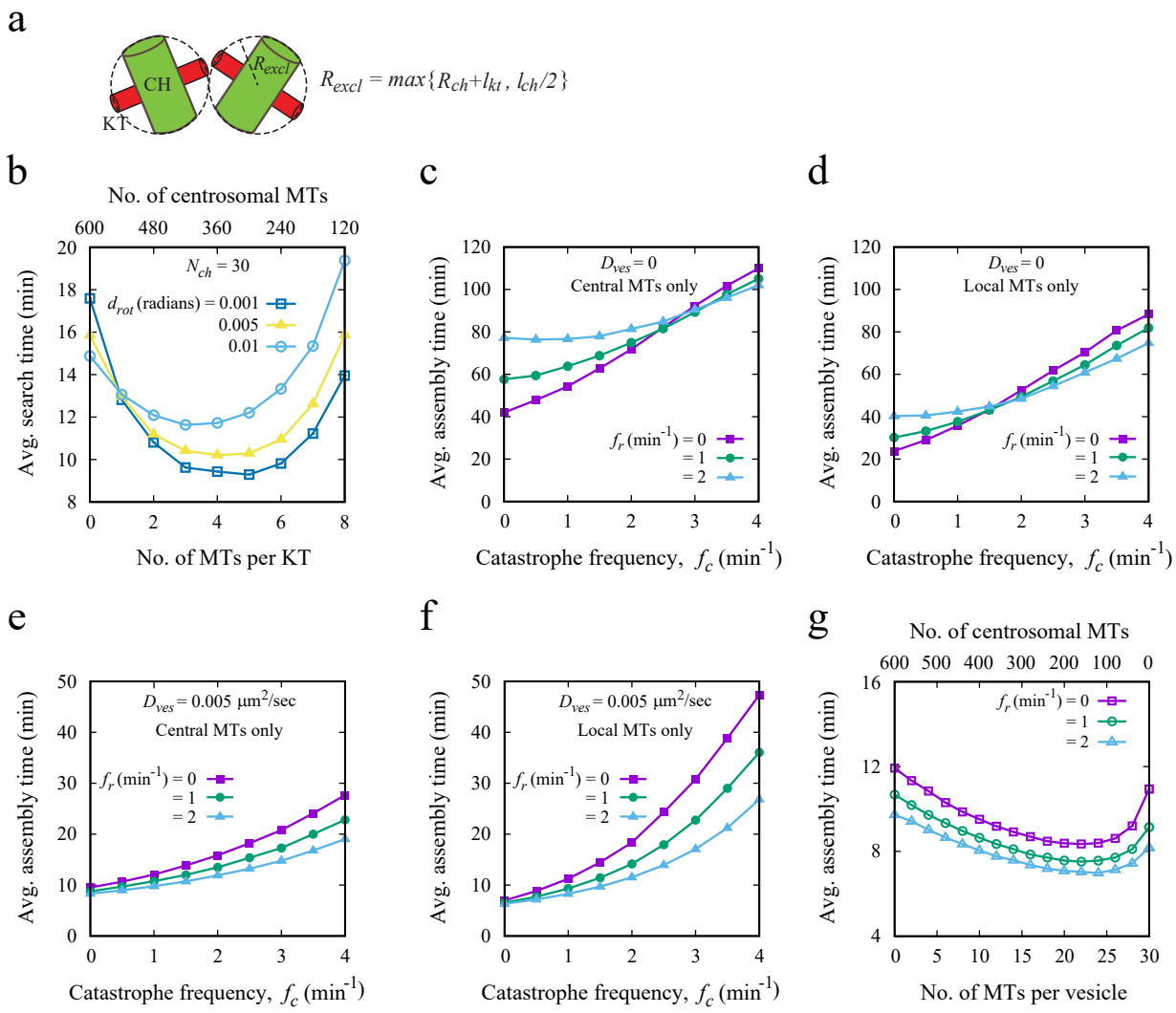

FIGURE S1 Model construction of chromosomal volume exclusion, impact of chromosomal rotation on average search time, and effect of microtubule (MT) rescue frequency on vesicle assembly. (*a*) Schematic depiction of chromosome exclusion in the model. A spherical exclusion zone is defined around each chromosome with radius $R_{excl} = max\{R_{ch} + l_{kt}, l_{ch}/2\}$, where R_{ch} and l_{ch} are the radius and length of the cylindrical chromosome (CH), and l_{kt} is the length of the associated kinetochore (KT) cylinder. The centers of two chromosomes are not allowed to come closer than $2R_{excl}$. (*b*) Average search time as a function of the number of MTs per KT for different rotational diffusion rates of chromosomes, determined by d_{rot}. Increasing d_{rot} enhances the rotational mobility of chromosomes. (*c–f*) Optimized rescue frequency (f_r) is sensitive to vesicle mobility and catastrophe frequency (f_c). (*c–d*) Zero rescue is optimal for static vesicles. (*e–f*) At higher vesicle mobility, a finite rescue frequency becomes more advantageous than zero rescue in reducing assembly time. At higher catastrophe frequencies, a non-zero rescue supports sustained MT growth toward vesicles, enhancing search efficiency even when vesicles are static (*c–f*). (*g*) Qualitative trends in assembly time remain similar across different rescue frequencies. Simulations were performed with a MT catastrophe frequency of $f_c = 0.016$ sec^{-1} and vesicle diffusion coefficient $D_{ves} = 0.005$ μm^2/sec. (*c–g*) Simulations were performed with $N_{ves} = 20$.

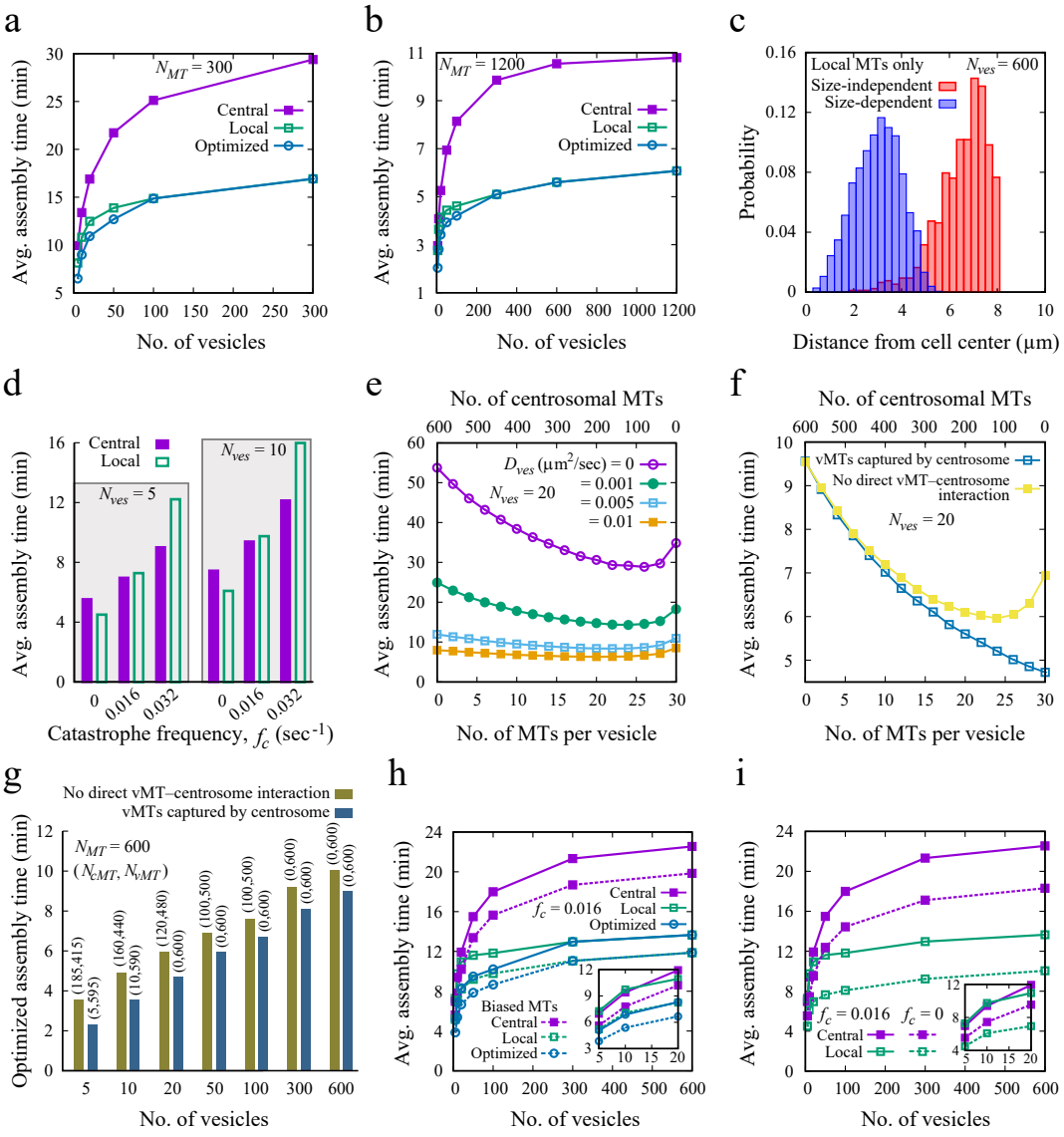

FIGURE S2 Effect of MT parameters, simulation conditions, and diffusion on vesicle assembly. (*a–b*) Assembly time for reduced (N_{MT} = 300, *a*) and increased (N_{MT} = 1200, *b*) total MTs, relative to the default (N_{MT} = 600). MTs grow without spontaneous catastrophe (f_c = 0) inside the cell. (*c*) The distance of the final vesicle aggregate from the cell center shows that, without central MTs, vesicles assemble within the cell interior, away from the center. Simulations were performed under two conditions: (i) Size-independent merging — the merged vesicle positions near either of the original vesicles, regardless of size (red bar), and (ii) Size-dependent merging — the merged vesicle settles near the larger one, resulting in a more inward position of the final aggregate (blue bar). Notably, average assembly times reported throughout the manuscript figures remain consistent across both scenarios. (*d*) Assembly time for N_{ves} = 5 and 10 with MTs assigned to central or local searchers, shown for f_c = 0, 0.016, and 0.032 sec^{-1}. (*e*) Assembly time decreases with increasing vesicle diffusion (N_{ves} = 20). (*c*, *e*) Simulations use f_c = 0.016 sec^{-1}. (*f–g*) Sensitivity of assembly to vesicular MT–centrosome interaction conditions. (*f*) Average assembly time as a function of the number of MTs per vesicle under two conditions: (i) vesicular MTs (vMTs) can interact with the centrosome, modeled as a sphere of radius 0.5 μm that captures vMTs upon contact; (ii) vMTs do not physically interact with the centrosome. (*g*) Optimized assembly time vs. vesicle number for both vMT-centrosome interaction and non-interaction scenarios. For 600 total MTs, optimal allocations to centrosomal (N_{cMT}) and vesicular MTs (N_{vMT}) are labeled above bars. (*f–g*) Simulations performed with f_c = 0. (*h*) Assembly time versus vesicle number for MT searchers assigned to central, local, or as per optimized combinations. Simulations use uniform catastrophe (f_c = 0.016 sec^{-1}) and biased MTs ($d_{stab} = R_c/4$, α = 10). (*i*) Comparison of uniform catastrophe (f_c = 0.016 sec^{-1}) and no catastrophe inside the cell. (*a–e*, *h–i*) Simulations do not consider direct vMT–centrosome interaction.

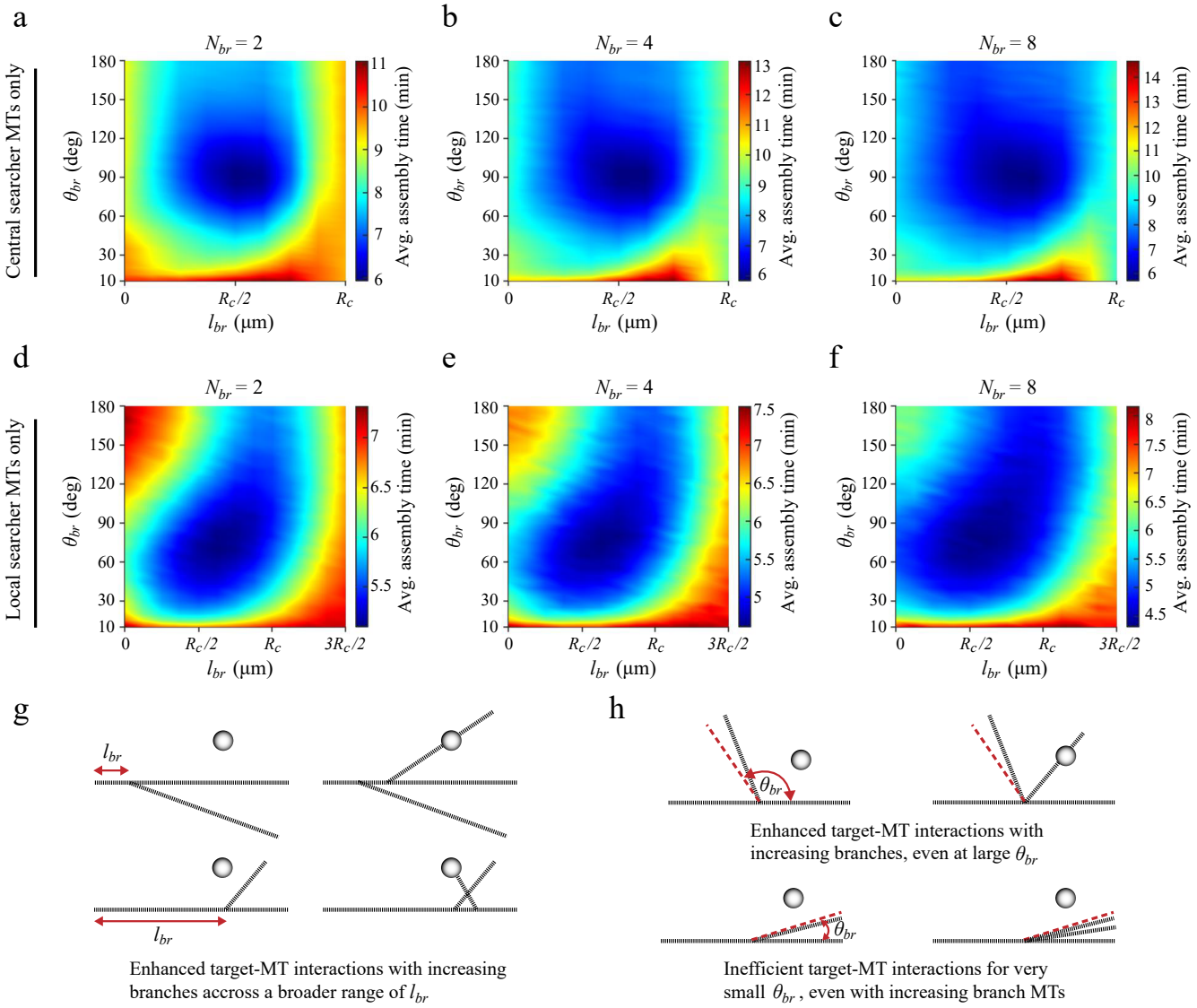

FIGURE S3 Vesicle assembly with varying numbers of branched MTs. (*a–c*) Assembly time versus branch length (l_{br}) and angle (θ_{br}) for N_{ves} = 20 with N_{br} = 2, 4, and 8 MT branches, using only central searchers (N_{cMT} = 600). (*d–f*) Similar analysis with all MTs as local searchers (N_{vMT} = 600). (*g*) Schematic showing that increasing MT branches expands the search area, improving MT-vesicle encounters across a wider range of l_{br}. (*h*) At larger θ_{br}, more branches enhance MT-vesicle interactions, while very small θ_{br} limits coverage and reduces assembly efficiency. Schematics in (*g*) and (*h*) are simplified representations of the underlying 3D geometry.

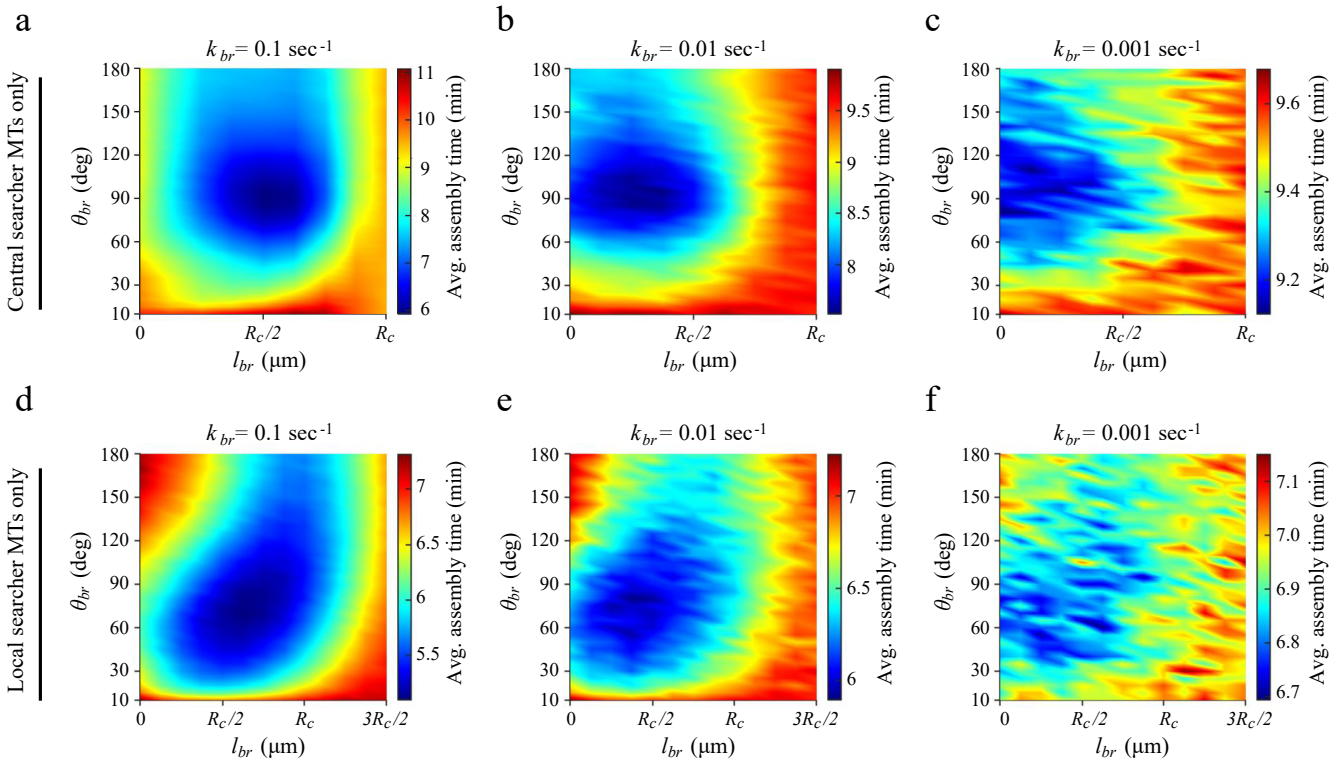

FIGURE S4 Vesicle assembly time across varying MT branching rates. Average assembly time as a function of l_{br} and θ_{br} for N_{ves} = 20 at branching rates k_{br} = 0.1, 0.01, and 0.001 sec^{-1}, with MTs assigned to central searchers (N_{cMT} = 600, *a–c*) or local searchers (N_{vMT} = 600, *d–f*).

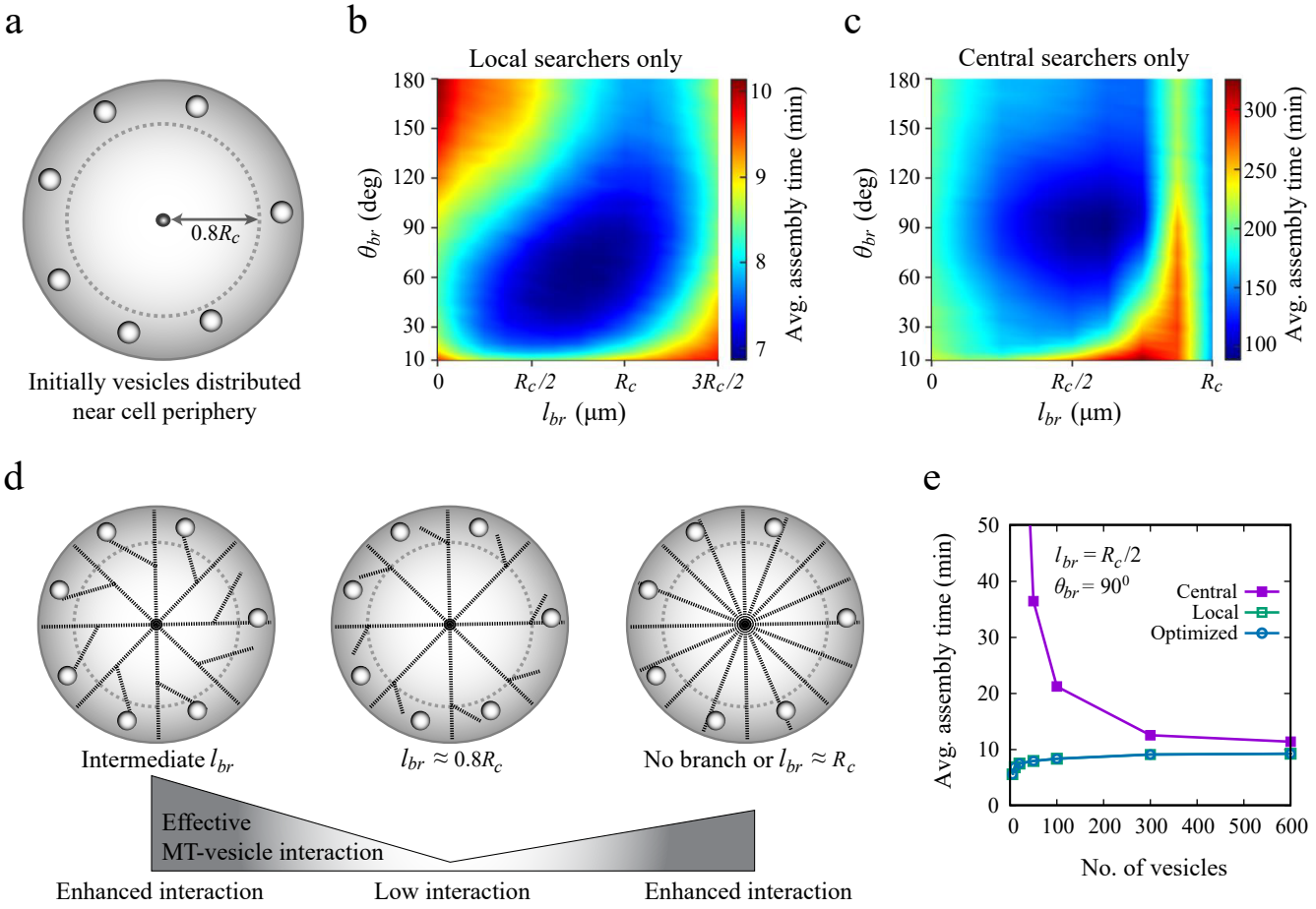

FIGURE S5 Vesicle assembly with peripheral vesicle distribution. (*a*) Vesicles are placed in an annular region of width $0.2R_c$ near the cell periphery. (*b–c*) Average assembly time as a function of branching length (l_{br}) and angle (θ_{br}) for $N_{ves} = 20$, with MTs assigned to local searchers ($N_{vMT} = 600$, *b*) or central searchers ($N_{cMT} = 600$, *c*). (*d*) Schematic, representing a simplified view of the underlying 3D geometry, showing reduced MT-vesicle interactions for $l_{br} \approx 0.8R_c$ compared to intermediate ($l_{br} \approx R_c/2$) or larger values ($l_{br} \approx R_c$). For $l_{br} \approx R_c$, mother central searcher MTs grow close to the cell periphery, nullifying branching effects and aligning with the no-branching scenario. (*e*) Average assembly time vs. vesicle number for $l_{br} = R_c/2$ and $\theta_{br} = 90°$, comparing MTs exclusively assigned to central searchers, local searchers, or an optimized combination of both, yielding minimal assembly time.

Supplemental Table

TABLE S1 List of variables used in the model

Abbreviations	Meaning	Value | Range | Reference
R_c	Cell radius	10 µm
R_{ves}	Initial vesicle radius	0.25 µm
N_{ves}	Number of initial vesicles	5 – 600
N_{ch}	Number of chromosomes	5 – 50
N_{kt}	Number of kinetochores	10 – 100
R_{ch}	Chromosome radius	0.7 µm
l_{ch}	Chromosome length	2 µm | (1)
R_{kt}	Kinetochore radius	0.44 µm | (1)
l_{kt}	Kinetochore length	0.35 µm | (1)
D_{ves}	Effective diffusion constant of the initial vesicles	0.005 $\mu m^2/sec$ | 0.001 – 0.01 $\mu m^2/sec$
D_{ch}	Effective diffusion constant of the chromosomes	0.005 $\mu m^2/sec$ | (1)
N_{MT}	Total number of searcher MTs	600 | 300 – 1200
N_{br}	Number of MT branches per MT	2 | 2 – 8
k_{br}	Rate of branch initiation	0.1 sec^{-1} | 0.001 – 0.1 sec^{-1}
l_{br}	Cut-off distance for the branching MT nucleation	$0 - 3R_c/2$
θ_{br}	Angle between the branch MTs and the mother central or local searcher MTs	10° – 180°
d_{stab}	Distance that determines the span of the stabilizing gradients centered around each vesicle	$R_c/8, R_c/4, R_c$
α	A phenomenological constant determining the sensitivity of the catastrophe frequency to the stabilizing agents	0 – 50
v_g	MTs growth velocity	0.2383 µm/sec | (2)
v_s	MTs shrinkage velocity	0.2667 µm/sec | (2)
f_c	MTs catastrophe frequency	0 or $v_g/1.5R_c$ ($\approx 0.016\ sec^{-1}$) | (3)
f_r	MTs rescue frequency	0 | (3–5)

Supplemental Methods

Microtubule dynamics

Each microtubule (MT) is modeled as a cylindrical rod with a diameter of 25 nm and exhibits dynamic instability characterized by four parameters: growth velocity (v_g), shortening velocity (v_s), catastrophe frequency (f_c), and rescue frequency (f_r). During the growth phase, MTs elongate at velocity v_g until a catastrophe occurs at rate f_c, initiating a shortening phase with velocity v_s. A nonzero rescue frequency f_r can return a shortening MT to the growth phase.

In the simulations, rescue events are excluded ($f_r = 0$) for simplicity. Prior studies with static targets indicate that finite rescue increases search time by causing MTs to repeatedly grow in the same direction without a target there, prolonging futile searches (3–6). While zero rescue may optimize search efficiency for static or slowly diffusing targets, rescue events can accelerate assembly when targets exhibit higher diffusivity. Two scenarios were tested: (i) static vesicles (Figure S1, *c* and *d*) and (ii) diffusive vesicles with $D_{ves} = 0.005\ \mu m^2/sec$ (Figure S1, *e* and *f*). For static vesicles, the average search time is minimized at zero rescue frequency up to a certain threshold in catastrophe frequency. Beyond this threshold, a finite rescue frequency sustains MT growth toward the vesicle and enhances assembly efficiency. In contrast, for diffusive vesicles, increasing the rescue frequency consistently reduces the search time, even at low catastrophe rates. When the catastrophe frequency approaches zero, variations in rescue frequency have minimal influence on the search time for diffusive vesicles (Figure S1, *e* and *f*). Thus, setting $f_r = 0$ in simulations with zero or low catastrophe is justified, as the qualitative trends in assembly time remain robust across different rescue frequencies (Figure S1 *g*).

The dynamics of individual MTs were simulated using a Monte Carlo algorithm. At each time step Δt, a uniform

random number between 0 and 1 was drawn and compared to the transition probability from growth to shortening, given by $1 - \exp(-f_c \Delta t)$. If the random number was below this threshold probability, the MT transitioned to the shortening state. Once an MT fully shortened back to the origin, a new growth cycle began, with the MT nucleating in a randomly chosen direction.

Furthermore, the model assumes that MTs undergo rapid catastrophe upon contacting the chromosome arms or the cell membrane. This assumption is motivated by experimental observations: in vitro, MTs have been shown to rapidly catastrophe upon encountering a wall, likely due to the buildup of compressive forces at the growing tip (7). Similarly, in vivo studies report increased catastrophe rates when MTs contact cellular structures such as the plasma membrane (8), cortex (including transient dynein interactions) (9), or spindle pole bodies (10). Extrapolating from these findings, the model assumes a similar response upon MT contact with chromosome arms. While there may be brief periods of physical interaction before catastrophe (7)—during which MTs can exert pushing forces or engage with chromokinesins—such short-lived events are neglected in the current modeling framework to maintain simplicity.

Introduction of bias in MT dynamics

To compute the spatial bias of the MT dynamics near the vesicles, the spatial gradient of a stabilizing factor is modeled as a linear superposition of exponential decay functions centered at each vesicle (3):

$$G_i = \sum_{k=1}^{N_{ves}} \frac{v_k}{v_{tot}} \exp\left(-\frac{d_{ik}}{d_{stab}}\right) \tag{S1}$$

Here, v_{tot} is the volume of all vesicles, and v_k is the volume of the k-th vesicle, so larger vesicles generate stronger gradients. d_{ik} is the distance between the tip of the i-th MT and the center of the k-th vesicle. The decay length d_{stab} determines how rapidly the influence of each vesicle decreases with distance.

The catastrophe frequency for the i-th MT then becomes:

$$f_c^i = f_c \exp(-\alpha G_i) \tag{S2}$$

Here, f_c is the unbiased catastrophe frequency, and parameter α controls the MT's sensitivity to the stabilizing agents. As the value of parameter α increases, MTs become more sensitive to the bias, and the catastrophe frequency drops more steeply closer to the vesicles, vanishing right near the vesicles.

The same framework is applied to study the role of the RanGTP gradient in chromosomal assembly during mitosis.

Kinetics of Vesicles

Initially, small spherical vesicles are randomly distributed within the cellular volume. The position of each vesicle, $\mathbf{r}$ $(x_{ves}, y_{ves}, z_{ves})$, evolves over time t according to

$$\frac{d\mathbf{r}(t)}{dt} = \sqrt{2D_{ves}}\,\boldsymbol{\eta}(t), \tag{S3}$$

where D_{ves} is the diffusion coefficient of the vesicle. The components of the three-dimensional random vector $\boldsymbol{\eta}(t)$ $(\eta_1(t), \eta_2(t), \eta_3(t))$ follow a normal distribution with zero mean and unit variance. These components are statistically independent, satisfying $\langle \eta_i(t)\, \eta_j(t') \rangle = \delta_{ij}\, \delta(t - t')$, where $i, j = 1, 2, 3$, and δ_{ij} and $\delta(t - t')$ are the Kronecker and Dirac delta functions, respectively. Vesicle motion is confined to the interior of the cell by applying a reflecting boundary condition at the cell edge along the radial direction connecting the centers of the cell and vesicle.

Kinetics of Chromosomes

Initially, cylindrical chromosomes are randomly distributed within the cell, each with a random orientation. Orientation is defined using Euler angles ϕ_n $(n = 1, 2, 3)$, which allow full three-dimensional rotation of the chromosome along with its two associated cylindrical kinetochores. Chromosomes undergo translational diffusion characterized by a diffusion coefficient D_{ch}. At each computational time step, a random position is selected for each chromosome using an equation analogous to Eq. S3. If the proposed position overlapped with another chromosome, the move was rejected. To prevent such overlaps, a spherical exclusion zone is defined around each chromosome with radius $R_{excl} = max\{R_{ch} + l_{kt}, l_{ch}/2\}$, where R_{ch} and l_{ch} are the radius and length of the cylindrical chromosome, and l_{kt} is the length of the associated kinetochore cylinder. If two exclusion zones overlapped, the move was disallowed, and a new random position was chosen until a non-overlapping configuration was found. This particular choice of R_{excl} ensures that two chromosomes do not physically overlap during their rotational motion

within the spherical volume (see Figure S1 *a*). Additionally, if a proposed chromosome position lies outside cell boundary, it is reflected back into the cell interior to a position located at a distance, R_{excl}, away from the boundary, along the radial direction connecting the centers of the cell and chromosome. If the reflected position also results in an overlap, a new non-overlapping position is resampled.

At each computational time step Δt, chromosomes also undergo rotational diffusion. This is modeled by applying small-angle rotations to the Euler angles:

$$\phi_n(t + \Delta t) = \phi_n(t) + d_{\text{rot}}\,\mathcal{N}(0, 1), \quad n = 1, 2, 3, \tag{S4}$$

where $\mathcal{N}(0, 1)$ denotes a normally distributed random variable with mean zero and unit variance, sampled independently for each ϕ_n. The prefactor, $d_{\text{rot}} = 0.005$ radians, sets the typical magnitude of the rotational step. The choice of this value is somewhat arbitrary but was made to ensure that rotational motion does not dominate the overall capture kinetics. Excessive rotational mobility can increase the search time, particularly in the presence of kinetochore MTs, by inducing abrupt reorientations of the kinetochore MT array. This, in turn, can reduce the likelihood of productive interactions with centrosomal MTs and lead to inefficient capture (Figure S1 *b*).

Notably, the model adopts a simplifying assumption that each chromosome continues to undergo effective translational and rotational diffusion even after one or both kinetochores have been captured and connected to the spindle pole(s). In reality, post-attachment dynamics are influenced by multiple factors, including polymerization forces from growing MTs, polar ejection forces acting on chromosome arms, and motor activity at MT–chromosome interfaces (11, 12). Given that MTs can approach chromosomes from a wide range of angles, the resulting forces may still produce an overall effective diffusive behavior. Additionally, chromosome movements during prometaphase involve a complex interplay of motor proteins such as dynein/dynactin (13), CENP-E (14), and chromokinesins (15). The nature of the attachment — whether syntelic (both kinetochores are connected to the same centrosomal spindle pole via MTs), amphitelic (sister kinetochores are connected to opposite spindle poles), or merotelic (a single kinetochore is connected to both poles) — also significantly affects motion. As the precise characteristics of post-attachment chromosome dynamics remain incompletely understood, maintaining effective diffusion provides a tractable approximation that allows the model to remain focused on the kinetics of search and capture.

Capture conditions

The successful capture of target vesicles (or kinetochores in mitotic spindle assembly) by searcher MTs from different origins can occur either through end-on attachment at the MT tip or lateral contact along the MT surface. According to the classical *search and capture* model, static targets can only be captured when the growing MT tip encounters them directly. In contrast, mobile targets such as vesicles or kinetochores typically form attachments through lateral interactions as they move within the cell and come into contact with existing MTs, often aided by motor proteins.

At each computational time step, end-on capture is evaluated by measuring the shortest distance between the MT tip and the center of the vesicle (or the axis of the kinetochore cylinder in chromosome models). If this distance is less than the radius of the target, capture is considered successful. For lateral capture, the shortest distance between the vesicle center (or kinetochore axis) and the MT axis is computed. A target is captured laterally if this distance is less than the sum of the MT and target radii.

The model does not include any steric (excluded volume) interactions between MTs by default. However, in simulations that include inter-MT crosslinking, two MTs from different origins can interact by capturing each other at a rate $k_{\text{inter-MT}}$, provided their shortest inter-axial distance is less than the combined radii (each MT has a radius of approximately 12.5 nm). If an MT associated with a vesicle or kinetochore is captured in this way, the corresponding target vesicle or kinetochore is also considered captured.

Supporting References

1. Paul, R., R. Wollman, W. T. Silkworth, I. K. Nardi, D. Cimini, and A. Mogilner, 2009. Computer simulations predict that chromosome movements and rotations accelerate mitotic spindle assembly without compromising accuracy. *Proc. Natl. Acad. Sci. USA.* 106:15708–15713.

2. Rusan, N. M., C. J. Fagerstrom, A.-M. C. Yvon, and P. Wadsworth, 2001. Cell Cycle-Dependent Changes in Microtubule Dynamics in Living Cells Expressing Green Fluorescent Protein-α Tubulin. *Mol. Biol. Cell.* 12:971–980.

3. Wollman, R., E. Cytrynbaum, J. Jones, T. Meyer, J. Scholey, and A. Mogilner, 2005. Efficient chromosome capture requires a bias in the 'search-and-capture' process during mitotic spindle assembly. *Curr. Biol.* 15:828–832.

4. Holy, T., and S. Leibler, 1994. Dynamic instability of microtubules as an efficient way to search in space. *Proc. Natl. Acad. Sci. USA.* 91:5682–5685.

5. Sarkar, A., R. Paul, and H. Rieger, 2019. Search and Capture Efficiency of Dynamic Microtubules for Centrosome Relocation during IS Formation. *Biophys. J.* 116:2079–2091.

6. Gopalakrishnan, M., and B. S. Govindan, 2011. A first-passage-time theory for search and capture of chromosomes by microtubules in mitosis. *Bull. Math. Biol.* 73:2483–2506.

7. Janson, M. E., M. E. de Dood, and M. Dogterom, 2003. Dynamic instability of microtubules is regulated by force. *J. Cell Biol.* 161:1029–1034.

8. Tran, P., L. Marsh, V. Doye, S. Inoue, and F. Chang, 2001. A mechanism for nuclear positioning in fission yeast based on microtubule pushing. *J. Cell Biol.* 153:397–412.

9. Kozlowski, C., M. Srayko, and F. Nedelec, 2007. Cortical microtubule contacts position the spindle in C. elegans embryos. *Cell.* 129:499–510.

10. Tischer, C., D. Brunner, and M. Dogterom, 2009. Force-and kinesin-8-dependent effects in the spatial regulation of fission yeast microtubule dynamics. *Mol. Syst. Biol.* 5:250.

11. Dogterom, M., J. W. Kerssemakers, G. Romet-Lemonne, and M. E. Janson, 2005. Force generation by dynamic microtubules. *Curr. Opin. Cell Biol.* 17:67–74.

12. Brouhard, G. J., and A. J. Hunt, 2005. Microtubule movements on the arms of mitotic chromosomes: polar ejection forces quantified in vitro. *Proc. Natl. Acad. Sci. USA.* 102:13903–13908.

13. Vorozhko, V. V., M. J. Emanuele, M. J. Kallio, P. T. Stukenberg, and G. J. Gorbsky, 2008. Multiple mechanisms of chromosome movement in vertebrate cells mediated through the Ndc80 complex and dynein/dynactin. *Chromosoma.* 117:169–179.

14. Wood, K. W., R. Sakowicz, L. S. Goldstein, and D. W. Cleveland, 1997. CENP-E is a plus end–directed kinetochore motor required for metaphase chromosome alignment. *Cell.* 91:357–366.

15. Mazumdar, M., and T. Misteli, 2005. Chromokinesins: multitalented players in mitosis. *Trends Cell Biol.* 15:349–355.